Fluorescence and REMPI Spectroscopy of Jet-Cooled Isolated 2-Phenylindene in the S_1 State

Christian Müller,*,† Michael Klöppel-Riech,‡ Frauke Schröder,‡ Jörg Schroeder,†,‡ and Jürgen Troe†,‡

Institut für Physikalische Chemie der Universität, Tammannstr. 6, D-37077 Göttingen, Germany, and Abteilung Spektroskopie und Photochemische Kinetik, Max-Planck-Institut für Biophysikalische Chemie, Am Fassberg, D-37077 Göttingen, Germany

Received: January 18, 2006; In Final Form: February 17, 2006

We investigated the spectroscopy of the first excited singlet electronic state S_1 of 2-phenylindene using both fluorescence excitation spectroscopy and resonantly enhanced multiphoton ionization spectroscopy. Moreover, we investigated the dynamics of the S_1 state by determining state-selective fluorescence lifetimes up to an excess energy of ~3400 cm^{-1}. Ab initio calculations were performed on the torsional potential energy curve and the equilibrium and transition state geometries and normal-mode frequencies of the first excited singlet state S_1 on the CIS level of theory. Numerous vibronic transitions were assigned, especially those involving the torsional normal mode. The torsional potentials of the ground and first excited electronic states were simulated by matching the observed and calculated torsional frequency spacings in a least-squares fitting procedure. The simulated S_1 potential showed very good agreement with the ab initio potential calculated on the CIS/6-31G(d,p) level of theory. TDDFT energy corrections improved the match with the simulated S_1 torsional potential. The latter calculation yielded a torsional barrier of $V_2 = 6708$ cm^{-1}, and the simulation a barrier of $V_2 = 6245$ cm^{-1}. Ground-state normal-mode frequencies were calculated on the B3LYP/6-31G-(d,p) level of theory, which were used to interpret the infrared spectrum, the FDS spectrum of the 0_0^0 transition and hot bands of the FES spectrum. The fluorescence intensities of the ν_{49} overtone progression could reasonably be reproduced by considering the geometry changes upon electronic excitation predicted by the ab initio calculations. On the basis of the torsional potential calculations, it could be ruled out that the uniform excess energy dependence of the fluorescence lifetimes is linked to the torsional barrier in the excited state. The rotational band contour simulation of the 0_0^0 transition yielded rotational constants in close agreement to the ab initio values for both electronic states. Rotational coherence signals were obtained by polarization-analyzed, time-resolved measurements of the fluorescence decay of the 0_0^0 transition. The simulation of these signals yielded corroborating evidence as to the quality of the ab initio calculated rotational constants of both states. The origin of the anomalous intensity discrepancy between the fluorescence excitation spectrum and the REMPI spectrum is discussed.

1. Introduction

The hindered internal rotation (torsion) about single bonds of nonrigid molecules possessing symmetric torsional double-minimum potential energy surfaces has gained increasing experimental[1−10] as well as theoretical[11−19] interest in the past two decades. In particular, the investigation under supersonic jet conditions has proven to be a viable way of obtaining detailed spectroscopic information for the determination of torsional potentials and torsional tunneling splittings in ground and excited electronic states. One of the rationales for investigating molecules possessing symmetric torsional double-minimum potentials lies in the possibility to test the applicability of quantum mechanical concepts and models in molecular physics. One may investigate one-dimensional model potentials, which serve to determine torsional tunneling splittings, the agreement between intensities of torsional progressions and calculated Franck−Condon factors, or the appropriateness of rigid-molecule point groups in the assignment and interpretation of spectra of molecules exhibiting large-amplitude low-frequency motions within multiple-minimum potentials.

Among the multitude of notable investigations on molecules with twofold torsional barriers, the publications on styrene dealing with the experimental[1,6,20] and ab initio[11−14,21−23] determination of the torsional potentials are particularly numerous. Other well-documented examples of this class of molecules are, e.g., tolane,[2] 9-phenylanthracene,[3] symmetrically substituted 9-phenylanthracenes,[4] 9-(*N*-carbazolyl)anthracene,[7,20] 2-phenylindole,[9,20] benzyl alcohol,[24] biphenyl[23,25,26] 9,9′-bianthryl,[5] and 2,2′-bipyrimidine.[27]

While numerous semiempirical and ab initio ground-state calculations for molecules possessing symmetric torsional double-minimum potentials can be found in the literature, e.g., for styrene,[11−14,21,22] biphenyl,[17,23] and polychlorinated biphenyls,[18] only few ab initio excited-state calculations are documented.[10,19,26,28−30] 2-Phenylindene (Figure 1) has gained little spectroscopic and dynamic interest in the past. Without exception, it has been treated as a torsionally hindered analogue of *trans*-stilbene, which, because of the methylene bridge

* Corresponding author. E-mail address: cmuelle4@gwdg.de.
† Institut für Physikalische Chemie der Universität.
‡ Max-Planck-Institut für Biophysikalische Chemie.

10.1021/jp060366j CCC: $33.50 © 2006 American Chemical Society
Published on Web 03/30/2006

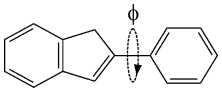

Figure 1. 2-Phenylindene and the torsional angle ϕ between the phenyl ring and the indene moiety.

forming the indene five-membered ring, cannot undergo the ethylenic torsion leading in the case of *trans*-stilbene to *cis*-stilbene. Instead, the torsion about the single bond connecting the phenyl ring with the indene moiety has been regarded as the reaction coordinate.[8,31]

A thorough investigation of fluorescence properties of 2-phenylindene under supersonic jet conditions was carried out by Heikal, Baskin, Bañares, and Zewail (HBBZ).[8] Qian, Schultz, and Jean[32] investigated intramolecular vibrational energy redistribution (IVR) and vibrational cooling of 2-phenylindene in hexane solution by picosecond time-resolved resonance Raman pump−probe spectroscopy. Dutt, Konitsky, and Waldeck[33] determined the fluorescence lifetimes of 2-phenylindene in different alkane solvents, methanol, and acetonitrile at different temperatures.

In this contribution, we present frequency-, time-, and polarization-resolved measurements of the $S_1 \leftarrow S_0$ electronic transition of 2-phenylindene. The frequency-resolved measurements comprise the fluorescence excitation spectrum (FES), the resonantly enhanced multiphoton ionization (REMPI) spectrum, and the rotational band contour of the 0_0^0 band origin. Fluorescence lifetimes τ_{fl} were obtained up to an excess energy of $\sim$3400 cm^{-1} from time-resolved fluorescence measurements with broad-band detection. The transients of the time-resolved, polarization-analyzed fluorescence measurements were interpreted as a manifestation of purely rotational coherence.

In an effort to assess the appropriateness of ab initio calculations carried out on the CIS level of theory to account for our spectroscopic and dynamic findings, we performed S_1-state calculations of the torsional potential energy curve and the equilibrium and transition-state geometries and normal-mode frequencies. Supported by the ab initio calculations, numerous vibronic transitions were assigned, especially those involving the torsional normal mode. The torsional potentials of the ground and first excited electronic states were obtained by matching the observed and calculated torsional frequency spacings in a least-squares fitting procedure. Moreover, the rotational band contour of the 0_0^0 band origin was simulated using the calculated S_0 and S_1 rotational constants.

2. Experimental Section

The details of the experimental setup for measuring fluorescence excitation spectra have been described elsewhere.[34,35] We therefore only summarize the main features. The jet apparatus consisted of a vacuum chamber evacuated by a diffusion pump (Edwards Diffstak 250/2000M) backed by a rotary pump (Edwards E2M40). The sample was heated to 110−120 °C, entrained in 3.5−4.0 bar helium, and expanded into the vacuum using a General Valve series 9 pulsed nozzle ($\varnothing = 100$ μm) operated at the repetition rate of the nanosecond laser system (10 Hz).

For the measurement of the medium-resolution fluorescence excitation spectrum (Figure 3), the jet beam was crossed at right angles by a parallel polarized laser beam. The nanosecond laser system consisted of a dye laser (Lambda Physik Scanmate II, 0.2 cm^{-1} resolution, 5−6 ns pulse duration) pumped by a Nd:YAG laser (Quantel Brilliant ω) at a 10 Hz repetition rate. The dye-laser beam was frequency doubled in a KDP crystal to generate excitation wavelengths in the range 293−319 nm. The horizontally expanding free jet was crossed by the laser beam at a distance of 8−10 mm from the nozzle. The broadband fluorescence from the interaction region of the crossed molecular and laser beams was collected at right angles to both beams by a *f*/1 collimating lens and focused by a second lens onto the entrance of a microchannel plate photomultiplier (MCP-PMT, Hamamatsu R3809U). The resulting signal was accumulated in a homemade boxcar integrator, digitized, and stored in a computer. The resulting fluorescence excitation spectrum was neither corrected for the spectral response of the detection system nor corrected for the power curve of the dye laser.

The fluorescence lifetimes were determined by time-correlated single-photon counting using a picosecond dye-laser system for excitation. The picosecond dye-laser system was also used for the measurement of a low-resolution fluorescence excitation spectrum (Figure 5). The picosecond laser system consisted of a free jet dye laser (Coherent CR 599) synchronously pumped by the frequency-doubled output of a Nd:YLF laser (Coherent Antares II, 527 nm, 30−50 ns pulse duration, 0.8−1.0 W) at a repetition rate of 76 MHz giving pulses with a duration of 5−10 ps at a bandwith of 1.5−3.0 cm^{-1}. The dye-laser beam was frequency-doubled in a BBO crystal (572−604 nm) or a $LiIO_3$ crystal (602−622 nm) to generate excitation wavelengths in the range 286−311 nm. Wavelength calibration was performed by optogalvanic spectroscopy with a neon discharge lamp. The laser beam crossed the continuous jet expansion about 4−6 mm downstream of the nozzle ($\varnothing = 75$ μm).

For time-correlated single-photon counting, the output of the MCP-PMT was amplified and fed into a constant fraction discriminator which delivered the start pulses for a time-to-amplitude converter (Tennelec TC 862) operated in reversed mode.[36] A second CFD provided the stop pulses which were derived from a photodiode monitoring the laser output. The full width at half-maximum (fwhm) of the instrument response function was usually about 150 ps. For the analysis of the fluorescence decay histograms, a Fourier transform-based convolution and fitting procedure employing the Levenberg−Marquardt algorithm was used.

For rotational coherence spectroscopy (RCS), a Glan-Taylor polarizer was inserted in front of the MCP-PMT. Measurements were carried out for analyzer polarization orientations parallel and perpendicular with respect to the incident laser beam polarization. With the rotational coherence measurements, neon was used as carrier gas at a pressure of $\sim$2 bar.

The REMPI apparatus has been described in detail elsewhere,[37,38] and only the relevant features are described here. The apparatus consisted of three basic components: the molecular beam and the vacuum system, the time-of-flight mass spectrometer, and the nanosecond laser system.

The molecular beam apparatus consisted of three expansion chambers. The first expansion chamber was pumped to a pressure of 10^{-6} mbar by a diffusion pump (Edwards EO400) backed by a combination of a rotary pump (Edwards E2M40) and a roots pump (Edwards EH250). The sample was heated to $\sim$120 °C, entrained in a mixture of 0.52% xenon in helium/neon (1:1) at a stagnation pressure of 2 bar, and expanded into the first expansion chamber using a General Valve series 9 pulsed nozzle ($\varnothing = 200$ μm) operated at the repetition rate of the nanosecond laser system (10 Hz). The free jet passed the first skimmer to form a molecular beam in the second expansion chamber, which was evacuated to a pressure of $<10^{-6}$ mbar by a diffusion pump (Edwards Diffstak 250/2000M) backed by a second rotary pump (Edwards E2M40). The second chamber

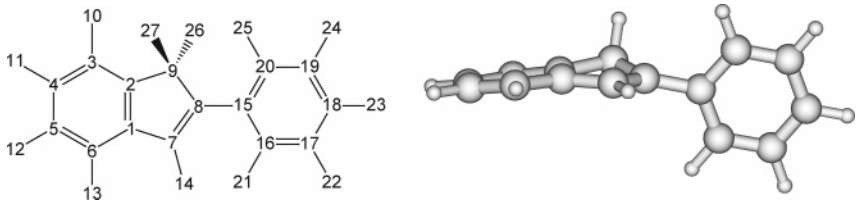

Figure 2. Atom labeling scheme and transition-state geometry of the S_1 state. The torsional angle $\phi = \angle(7, 8, 15, 16)$ has a value of $-90.5°$. The single imaginary frequency corresponding to the torsional motion of the phenyl ring around the indene moiety has a value of 96.1i cm^{-1} (unscaled).

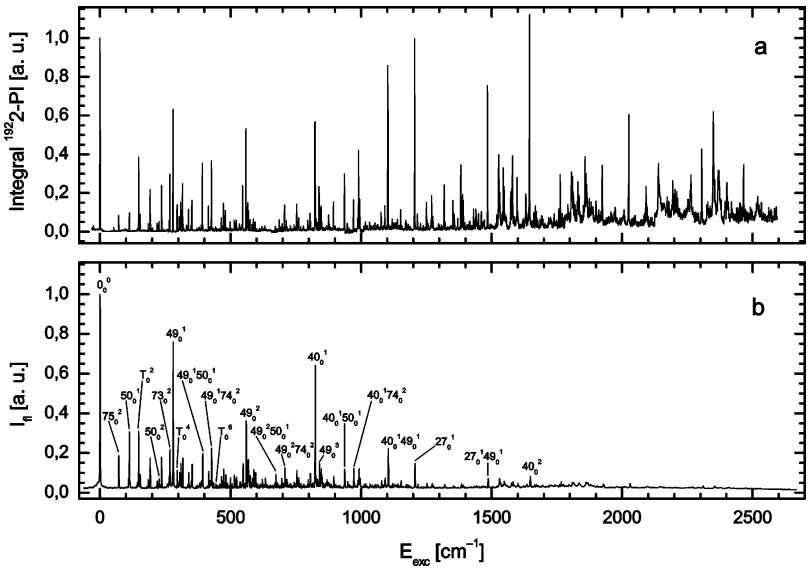

Figure 3. REMPI spectrum (a) and medium-resolution fluorescence excitation spectrum with assignment of some vibronic transitions (b).

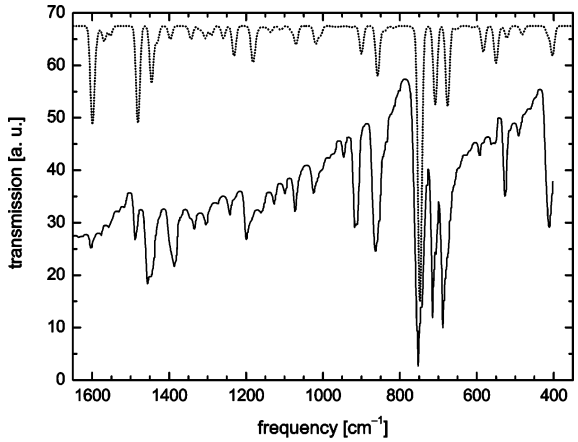

Figure 4. Infrared spectrum (full line) and calculated spectrum (dotted line, B3LYP/6-31G(d,p)). For a better visual comparison, the calculated spectrum was convoluted with a Gaussian line shape of fwhm = 5 cm^{-1}.

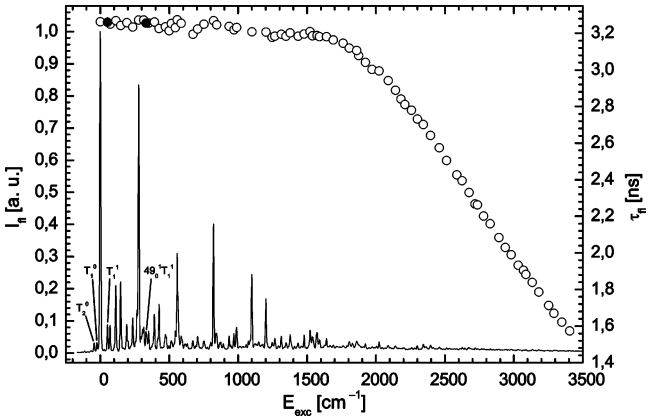

Figure 5. Low-resolution fluorescence excitation spectrum and energy dependence of the fluorescence lifetimes τ_{fl}. T_2^0, T_1^0, T_1^1, and $49_0^1T_1^1$ denote hot bands appearing under continuous expansion conditions.

contained at right angles the time-of-flight tube, which was evacuated to a pressure of 10^{-7} mbar by a turbomolecular pump (Seiko Seiki STP400) backed by the second rotary pump (Edwards E2M40). The third chamber was separated from the second chamber by a second skimmer.

The time-of-flight mass spectrometer consisted of a triple grid ion extraction region according to the setup of Wiley and McLaren,[39] a transverse field compensating for the transverse velocity of the ions resulting from the jet expansion, a focusing einzel lens, a 0.48-m-long drift tube, and a two-stage chevron microchannel plate detector (Galileo/Burle, active area $\varnothing = 25$ mm, gain 10^6-10^7). The fwhm of typical mass lines was in the range 8−11 ns.

For measuring the REMPI spectrum (Figure 3), the jet beam was crossed at right angles by the pulse train of a nanosecond laser system. This laser system consisted of a dye laser (Lambda Physik Scanmate II, <0.15 cm^{-1} resolution) pumped by a XeCl excimer laser (Lambda Physik LPX130i) at a repetition rate of 10 Hz. The dye-laser beam was frequency-doubled in a KDP crystal to generate excitation wavelengths in the range 293−330 nm. Wavelength calibration was performed with an interferometric calibration device (Burleigh Wavemeter WA-5500). The resulting REMPI spectrum was neither corrected for the spectral response of the detection system nor corrected for the power curve of the dye laser.

The infrared spectrum of Figure 4 was measured in KBr with a Perkin-Elmer IR-spectrometer (series FTIR1600).

2-Phenylindene was purchased from Aldrich and used without further purification.

3. Computational Details

All calculations were carried out using the *Gaussian 98* package of programs.[40] Ground-state geometry optimizations were carried out using a sequence of semiempirical (AM1) and Hartree−Fock (HF), Møller−Plesset perturbation theory (MP2), or density functional theory methods (B3LYP). Polarized and nonpolarized split valence basis sets (6-31G(d,p), 6-31G(d), and 6-31G) were used. The optimized ground-state geometries served as starting geometries for excited-state optimizations, which were carried out using the configuration interaction method with singly excited configurations (CIS) in combination with increasing polarized split valence basis sets (6-31G(d), 6-31G(d,p), 6-311G(d), and 6-311G(d,p)). Diffuse functions could not be used for the excited-state optimizations because of convergence failure of the optimization routine. All calculated geometries were checked to be minimum-energy geometries by subsequently calculating the corresponding normal-mode frequencies. The absence of any imaginary frequency indicated that a genuine minimum-energy geometry was found. The S_0 frequencies of Table VII (available as Supporting Information) calculated with the B3LYP/6-31G(d,p) method were scaled by a factor of 0.9613.[41,42] S_1 frequencies computed on the CIS level contain systematic errors because of the incomplete treatment of electron correlation as well as the neglect of vibrational anharmonicity. While there are a variety of publications dealing with the calculation of multiplicative frequency scaling factors, specific scaling factors, and linear scaling schemes for ground-state methods, as, e.g., for various semiempirical methods,[43−47] HF,[43,45−51] MP2,[43,45−51] diverse density functional theory (DFT) methods,[42−47,50−54] and QCISD[43,51] in combination with various basis sets, there is—to the best of our knowledge—so far no publication dealing with the calculation of scaling factors for frequencies calculated on the CIS level. Hence, with CIS being a Hartree−Fock-based method, a scaling factor of 0.8929 introduced by Pople[48] is used to compensate for these errors. The S_0 and S_1 normal modes of Table VII are numbered separately according to the numbering scheme of Mulliken[55] and Herzberg.[56]

Potential energy curves in the electronic ground state as well as in the first excited state were determined as a function of the torsional angle $\phi = \angle(7, 8, 15, 16)$ (for the atom labeling scheme, see Figure 2). Relaxed potential energy scans representing the adiabatic rotation of the phenyl and indene moieties against each other were carried out by increasing the torsional angle ϕ by steps of 10° and optimizing all other internal coordinates in every step. For the S_0 state, different ab initio and DFT methods were employed: HF, the local SVWN functional, and the hybrid functionals B3LYP, B3PW91, and MPW1PW91 in combination with the polarized split valence basis set 6-31G(d,p) and MP2 in combination with the simple split valence basis set 6-31G. For the S_1 state, the minimum-energy path (MEP) along the torsional coordinate was calculated with the CIS/6-31G(d,p) method. To account for dynamic electron correlation in the excited state, time-dependent density functional theory (TDDFT) energies were calculated for the CIS/6-31G(d,p)-MEP geometries.

Moreover, transition-state geometries were located in the S_0 and S_1 states, and transition-state frequencies were calculated. For the localization of the transition-state geometries, the synchronous transit-guided quasi-Newton method (STQN)[57,58] was employed (QST2 keyword in Gaussian) together with the B3LYP/6-31G(d) level of theory for the S_0 state and with the CIS/6-31G(d) level of theory for the S_1 state.

TABLE 1: Torsional Angles ϕ Calculated for the S_0 and S_1 State

	method	torsional angle ϕ
S_0	AM1	0
	HF/6-31G(d)	23.1
	MP2/6-31G	33.9
	B3LYP/6-31G(d)	0
	B3LYP/6-31G(d,p)	0
S_1	CIS/6-31G(d)	0
	CIS/6-31G(d,p)	0
	CIS/6-311G(d)	0
	CIS/6-311G(d,p)	0

Finally, in an attempt to account for the intensity anomaly between the REMPI spectrum and the fluorescence excitation spectrum to be discussed in the following section, vertical and adiabatic ionization energies were calculated. For the calculation of the vertical ionization energy, restricted outer valence Green's function (OVGF)[59−64] calculations were carried out. For this purpose, the basis sets 6-31G, 6-31G(d), and 6-31G(d,p) were used. The adiabatic ionization energy was calculated as the energy difference between the equilibrium geometries of the neutral 2-phenylindene molecule (restricted B3LYP) and the singly charged 2-phenylindene cation (unrestricted B3LYP). The RB3LYP energy of the neutral molecule and the UB3LYP energy of the cation were calculated with the basis sets 6-31G(d), 6-311G(d), and 6-311++G(d,p). Zero-point energy corrections were not taken into account.

4. Results and Discussion

4.1. Spectroscopy. *4.1.1. Fluorescence Excitation Spectrum and REMPI Spectrum.* For an assignment of fluorescence excitation and REMPI spectra of 2-phenylindene, it is of crucial importance to determine the symmetry of the nuclear configurations in both electronic states involved in the electronic transition. As can be seen in Figure 1, highest-symmetry equilibrium conformations of C_s point group symmetry can be expected for a torsional angle of $\phi = 0$. The torsional angle of the equilibrium conformation of a given electronic state depends on the competition between π-conjugation stabilizing an C_s equilibrium conformation and steric hindrance between nonbonded atoms favoring an equilibrium geometry without mirror symmetry. In an attempt to account for these subtle interactions theoretically, ab initio calculations were performed on the equilibrium geometries of both electronic states.

In Table 1, the torsional angles of the ground electronic state S_0 and the first excited electronic state S_1 calculated on different levels of theory are given. While our CIS computations clearly favor C_s point group symmetry for the S_1 state, the results on the S_0 equilibrium conformation are ambiguous. We, however, prefer the C_s point group conformation obtained with the B3LYP method for two reasons.

First, on theoretical grounds, our findings concerning the S_0 torsional angle of 2-phenylindene calculated on the Hartree−Fock and Møller−Plesset levels of theory, 23° and 34°, respectively, are in agreement with previous findings for molecules possessing comparable phenyl ring torsional coordinates, as, e.g., styrene and *trans*-stilbene. Numerous HF calculations with different basis sets on the S_0 equilibrium conformation of styrene gave torsional angles between 19° and 25°.[12,13,21] In the case of *trans*-stilbene, torsional angles between 15° and 27° were calculated on the HF level of theory.[65−67]

On the other hand, also in agreement with our findings, all DFT calculations on the S_0 equilibrium geometries of *trans*-stilbene and styrene carried out with the BLYP, B3LYP, and

BVWN functionals in combination with different basis sets furnished planar conformations.[22,68]

In contrast to previous assessments, which either favored the MP2 computations[22] by comparing the calculated S_0 torsional angles with their experimental counterparts obtained from gas-phase electron diffraction studies,[69] or which tried to reconcile the HF and MP2 calculations with experimental findings from X-ray diffraction[70] and supersonic jet studies[71−74] by invoking intermolecular interactions or effective planarity due to very low torsional barriers,[13,14,22,65,67] we prefer our and previously reported DFT calculations. With regard to the correctness of the torsional angle, there is overwhelming evidence obtained from supersonic jet studies[1,71−75] in favor of planar S_0 equilibrium geometries for both *trans*-stilbene and styrene. Moreover, as will be shown below, the S_0 fundamental frequencies observed in the infrared spectrum of 2-phenylindene are in better agreement with the normal-mode frequencies calculated on the B3LYP/6-31G(d,p) level of theory than with those obtained from the HF/6-31G(d) and MP2/6-31G calculations.

Further, on spectroscopic grounds, the overall shape of the fluorescence excitation spectrum shown in Figure 3 does not suggest strong conformational changes upon electronic excitation from the ground state to the first excited state. The FES spectra of nonrigid molecules undergoing strong torsional changes upon electronic excitation exhibit long, bell-shaped intensity distributions which are attributed to torsional progressions.[2−5,7,9,20,25,26] For example, the FES spectrum of 2-phenylindole[9] has its most intense transition, which is attributed to the seventh torsional quantum in the S_1 state, at an excess energy of 457 cm^{-1}. The torsional potentials of the S_0 and S_1 states were determined to have their minima at 27° and 0°, respectively.

In contrast, nonrigid molecules, as, e.g., styrene[73] and tolane,[2] which undergo only slight conformational changes upon electronic excitation exhibit FES spectra of similar overall shape to that of 2-phenylindene.

The foregoing can be summarized as providing spectroscopic and theoretical support in favor of our hypothesis that 2-phenylindene has C_s point group symmetry in both electronic states. The rest of this section is devised to give conclusive quantitative support for our hypothesis. Furthermore, the ab initio calculations of the equilibrium conformations, normal-mode frequencies, torsional potentials, and transition-state geometries are tested as to their appropriateness to give a consistent picture of the spectroscopic properties studied in our work.

The reliability of the S_0 normal-mode frequencies calculated on the B3LYP/6-31G(d,p) level of theory was tested by comparison with experimental frequencies obtained from three types of sources: the hot bands of the low-resolution fluorescence excitation spectrum (Figure 5) and the transitions of the fluorescence dispersion spectrum of the 0_0^0 band reported by HBBZ[8] in the case of the low-frequency normal modes and the infrared spectrum (Figure 4) in the case of the high-frequency normal modes.

As is clearly discernible in Figure 4, there is very good agreement between the S_0 normal-mode frequencies calculated on the B3LYP/6-31G(d,p) level of theory and the frequencies of the observed IR transitions. Even the IR transition intensities are reasonably reproduced on the B3LYP/6-31G(d,p) level of theory, the most obvious deviations occurring for frequencies of >1300 cm^{-1}. A comparison of the experimental IR frequencies and the calculated S_0 normal-mode frequencies is given in Table VIII (available as Supporting Information). The IR spectra obtained from the HF/6-31G(d) and MP2/6-31G calculations are of poorer quality and are therefore not given here.

TABLE 2: Assignment for the Fluorescence Dispersion Frequencies [cm^{-1}] Relative to the 0_0^0 Band Origin

ν_{FDS}[a]	I_{FDS}[a]	assignment
0	100	0_0^0
46	17	75_2^0
96	4	75_4^0
117	12	74_2^0, 50_1^0
157	2.5	$74_2^075_2^0$, $50_1^075_2^0$
233	1.2	74_4^0, 50_2^0
283	63	49_1^0
325	14	$49_1^075_2^0$
374	4	$49_1^075_4^0$
399	7	$49_1^074_2^0$, $49_1^050_1^0$
435	2	$49_1^074_2^075_2^0$, $49_1^050_1^075_2^0$
515	1	$49_1^074_4^0$, $49_1^050_2^0$
563	22	49_2^0
604	13	$49_2^075_2^0$
650	2.5	$49_2^075_4^0$
677	4	$49_2^074_2^0$, $49_2^050_1^0$
715	3	$49_2^074_2^075_2^0$, $49_2^050_1^075_2^0$
841	9	49_3^0
870	40	40_1^0
880	13	$49_3^075_2^0$
908	6	$41_1^075_2^0$

[a] From ref 8.

TABLE 3: Experimental Frequencies ν_{FDS} of the Fluorescence Dispersion Spectrum of the 0_0^0 Transition and Frequencies ν_{calc} Calculated on the B3LYP/6-31G(d,p) Level of Theory[a]

ν_{FDS}[b]	ν_{calc} [cm^{-1}]	$\Gamma_j^{(1)}(l_i')$	S_0 normal mode
23.0	16.0	a″	ν_{75}
58.5	60.6	a″	ν_{74}
117	112	a′	ν_{50}
283	274	a′	ν_{49}
870	855	a′	ν_{40}

[a] The experimental value tabulated for ν_{74} was calculated to be half of the frequency value (117 cm^{-1}) observed in the FDS spectrum. [b] From ref 8.

With calculated S_0 normal-mode frequencies at hand, the fluorescence dispersion spectrum of the 0_0^0 band studied by HBBZ[8] was reassigned. The assignment of the reported transitions is given in Table 2.

From this assignment, the S_0 frequencies of at least three low-frequency normal modes could be determined (ν_{75}, ν_{49}, and ν_{40}; see Table 3). The comparison of the motional character of these normal modes with those of the previous assignment,[8] which was based on the normal-mode numbering scheme of *trans*-stilbene and on resemblance concerning the motional character of the normal modes of *trans*-stilbene and 2-phenylindene, shows that only the reassignment of ν_{25} from HBBZ[8] to ν_{49} in our present analysis implies a considerable difference in motional character. Normal-mode ν_{25} of *trans*-stilbene is a totally symmetric $C_e-C_e-\phi$ bending mode,[76] whereas ν_{49} of 2-phenylindene is a totally symmetric stretching mode. The normal modes ν_{75} and ν_{74} of 2-phenylindene, on the other hand, resemble ν_{37} and ν_{36} of *trans*-stilbene, respectively. The assignment of ν_{40} renders the tentative assigment X_n^0 of HBBZ[8] more precisely. The assignment of the transition at 117 cm^{-1} and progressions thereon, however, are ambiguous, since two different transitions (74_2^0 and 50_1^0) match the observed frequency spacing almost equally well.

The fluorescence excitation spectrum of Figure 5 provides corroborating evidence for the correctness of the assignment of

the S_0 normal mode ν_{75}. With the normal mode having the lowest frequency in the S_0 state, the torsional mode bears number 75 according to the normal-mode numbering scheme of Mulliken[55] and Herzberg.[56] In the S_1 state, however, the torsional mode bears number 74, as in this electronic state the lowest-frequency normal mode is a butterfly motion (see Figure I, available as Supporting Information).

We decided to apply separate normal-mode numbering schemes to both electronic states, thus circumventing difficulties concerning the motional character and the numbering of other normal modes arising from possible Duschinsky rotations.[77] For convenience, we simply labeled transitions involving the torsional normal mode as T_m^n, where m and n denote the number of torsional quanta in the ground and excited electronic state, respectively. Thus, the transitions labeled T_1^0 and T_2^0 in Figure 5 appearing at excess energies of -24.7 cm^{-1} and -44.9 cm^{-1}, respectively, are identical to the merely differently labeled transitions 75_1^0 and 75_2^0. The frequency spacings of the T_2^0 transition obtained from the FDS ($\nu_{FDS}(T_2^0) = 46$ cm^{-1}) and FES ($\nu_{FES}(T_2^0) = 44.9$ cm^{-1}) spectra are in excellent agreement. Additionally, the FES spectrum furnishes the S_0 fundamental frequency $\nu(T_1^0) = 24.7$ cm^{-1} of the torsional normal mode, which can directly be compared to the calculated value of 16.0 cm^{-1} (Table 3). The appearance of this hot band T_1^0, however, is quite exceptional, as it is a transition originating in the fundamental of the nontotally symmetric torsional normal mode under C_s point group restriction. Its presence can tentatively be rationalized as being due to large-amplitude torsional motion in the first torsionally excited state of the S_0 state resulting in effective nonplanarity and reduction of the point group symmetry to C_1 in the S_0 state.

The entire set of S_0 normal-mode frequencies calculated on the B3LYP/6-31G(d,p) level of theory is given in Table VII (available as Supporting Information) together with the S_1 normal-mode frequencies calculated on the CIS/6-31G(d,p) level of theory and the transition-state normal-mode frequencies of the S_0 and S_1 states calculated on the B3LYP/6-31G(d) and CIS/6-31G(d) levels of theory, respectively.

The orbital character of the $S_1 \leftarrow S_0$ electronic transition was calculated to have a dominant LUMO $\leftarrow$ HOMO contribution with an orbital coefficient of 0.6716 and a minor component with an orbital coefficient of 0.1028 arising from a LUMO + 3 $\leftarrow$ HOMO $-$ 3 contribution. The scalar product $\langle \mu | r^a \rangle$, with μ and r^a being unit vectors along the directions of the transition dipole moment and the a principal axis, is computed with the CIS/6-31G(d,p) method to have a value of 0.999. Hence, the transition dipole moment of the $S_1 \leftarrow S_0$ electronic transition is almost entirely long-axis (parallel) polarized. The electronic transition between the ground and first excited electronic states is of the type $\tilde{A}^1A' \leftarrow \tilde{X}^1A'$.

Because of the validity of the relations $A > B \approx C$ (Table 4), 2-phenylindene is a slightly asymmetric prolate top in both electronic states with small asymmetry parameters[56] in the ground state ($b'' = -8.03 \cdot 10^{-3}$) and the first excited state ($b' = -8.63 \cdot 10^{-3}$). According to the CIS/6-31G(d,p) calculations, the main conformational change upon electronic excitation is the shortening of the single bond (8, 15) connecting the indene moiety with the phenyl moiety (Figure 2) from 1.4666 Å in the S_0 state to 1.4067 Å in the S_1 state.

With 2-phenylindene possessing C_s point group symmetry in both the S_0 and S_1 states, the 75 vibrational modes factorize into 2 symmetry species: 50 totally symmetric a' modes ($\nu_1-\nu_{50}$) and 25 nontotally symmetric a'' modes ($\nu_{51}-\nu_{75}$). According to the electric dipole selection rules pertaining to FES and REMPI spectra, all fundamental, overtone, and combination bands are allowed for the a' modes, whereas for the a'' modes, only those overtone and combination bands with an even number of quanta are predicted to have nonvanishing intensities.[56] The assignment given in Table 5 was carried out with the S_1 normal-mode frequencies of Table VII calculated on the CIS/6-31G(d,p) level of theory. The restriction was imposed that 2-phenylindene possesses C_s point group symmetry in both electronic states.

TABLE 4: Comparison of the Rotational Constants [GHz] of the S_0 and S_1 States as Determined by the ab Initio Calculations and by Simulation of the Rotational Coherence Signals and the Rotational Band Contour of the 0_0^0 Transition

	ab initio	rotational contour	rotational coherence
S_0	B3LYP/6-31G(d,p)		
A	2.2755	2.2215	
B	0.2890	0.2884	
C	0.2569	0.2563	
B + *C*	0.5459	0.5447	
S_1	CIS/6-31G(d,p)		
A	2.2467	2.2093	
B	0.2957	0.2877	
C	0.2617	0.2607	
B + *C*	0.5575	0.5485	0.5499 ± 0.0077

The medium-resolution ($\sim$0.2 cm^{-1}) FES spectrum is given in Figure 3 together with the labels of some of the most prominent transitions. From this assignment, the S_1 frequencies of 13 normal modes could be determined (ν_{75}, ν_{74}, ν_{73}, ν_{50}, ν_{49}, ν_{48}, ν_{47}, ν_{46}, ν_{44}, ν_{42}, ν_{41}, ν_{40}, and ν_{27}; see Table 6). The experimental values tabulated for the a' normal modes were calculated from their first overtones by dividing the observed frequency values by 2.

The assignment of the FES spectrum of 2-phenylindene, however, is not unproblematic. First, the prominent bands labeled as Fermi resonances could not be attributed to any definite, dipole-allowed fundamentals, overtones, or combination bands containing as many as three normal modes. Their origin is unclear.

Second, the transitions labeled (192) and (236) could be the fundamentals of the S_1 normal modes ν_{72} and ν_{71}, respectively. As they are normal modes of a'' symmetry, neither their fundamentals nor the combination bands containing their fundamentals should possess any intensity according to the electric dipole selection rules. The alternative $73_0^1 75_0^3$ given for the (236) transition, being a combination band involving the change of four quanta in two normal modes, is unlikely to possess the high relative intensity given in Table 5. In the present framework, the assignment of the transitions at 192 and 236 cm^{-1} as being due to the fundamentals of a'' normal modes is only possible under the assumption that they are somehow induced transitions. Most obviously, they could be vibronically induced by Herzberg$-$Teller coupling.[78] In an attempt to clarify the possibility of Herzberg$-$Teller transitions, the symmetry species and vertical excitation energies of the lowest six excited singlet and triplet electronic states were calculated on the CIS/6-31G(d) level of theory. As can be seen from Table 7, all electronic wave functions of the calculated excited states are totally symmetric. For the occurrence of a Herzberg$-$Teller transition, it is required that[79]

$$\Gamma(\psi_e^{(i)}) \otimes \Gamma(\psi_e^{(j)}) \supset \Gamma(Q_t) \qquad (1)$$

where $\Gamma(\psi_e^{(i)})$ is the symmetry species of the electronic wave function of the borrowing state, $\Gamma(\psi_e^{(j)})$ the symmetry species

TABLE 5: Assignment for the S_1 Fluorescence Excitation Frequencies [cm^{-1}] Relative to the 0_0^0 Band Origin at (31 409.4 ± 0.4) cm^{-1}, Whose Intensity Was Arbitrarily Set to 100

ν_{FES}	I_{FES}	assignment	ν_{FES}	I_{FES}	assignment
0	100	0_0^0	554.5	5	$47_0^1 75_0^2$
71.9	19	75_0^2	560.6	36	49_0^2
109.9	7	$75_0^1 74_0^1$	565.4	15	Fermi resonance?
112.9	31	50_0^1	567.5	17	Fermi resonance?
143.2	5	75_0^4	570.3	11	Fermi resonance?
147.7	31	74_0^2	583.3	7	50_0^1 2× (236)
181.1	3	$75_0^3 74_0^1$	585.6	6	$73_0^2 48_0^1$
185.1	7	$50_0^1 75_0^2$	589.0	12	44_0^1
192.3	17	(192)	593.6	6	$47_0^1 50_0^1$
213.1	3	75_0^6	595.9	10	$49_0^1 48_0^1$
219.1	6	$75_0^2 74_0^2$	618.7	4	$46_0^1 75_0^2$
226.1	7	50_0^2	633.3	7	$49_0^2 75_0^2$, 48_0^2
235.6	18	$73_0^1 75_0^3$, (236)	673.9	9	$49_0^2 74_0^2$
257.9	4	$75_0^1 74_0^3$	708.4	13	$49_0^2 74_0^2$
259.6	4	$50_0^1 74_0^2$	715.4	7	47_0^1 (236)
263.4	5	75_0^2 (192)	753.9	11	42_0^1
265.9	9	75_0^2 (192)	761.7	8	$47_0^1 49_0^1$
268.2	22	73_0^2	797.4	7	$47_0^1 48_0^1$
280.5	76	49_0^1	805.7	10	41_0^1
290.2	3	75_0^8	824.1	64	40_0^1
296.0	11	74_0^4	827.8	8	$46_0^1 49_0^1$, $49_0^2 73_0^2$
304.8	10	50_0^1 (192)	840.5	15	49_0^3
309.9	15	74_0^1 (236)	845.7	10	Fermi resonance?
317.4	17	48_0^1	847.8	12	Fermi resonance?
336.5	4	50_0^3	850.7	8	Fermi resonance?
339.8	10	$73_0^2 75_0^2$	895.2	8	$40_0^1 75_0^2$
349.4	6	50_0^1 (236)	937.5	12	$40_0^1 50_0^1$
352.9	14	$49_0^1 75_0^2$	972.3	12	$40_0^1 74_0^2$
381.7	5	$73_0^2 50_0^1$	990.2	6	42_0^1 (236)
383.7	4	2× (192)	992.3	12	$40_0^1 75_0^1 73_0^1$
388.0	6	$48_0^1 75_0^2$	996.5	7	41_0^1 (192)
393.3	20	$49_0^1 50_0^1$	1092.6	7	$40_0^1 73_0^2$
410.3	3	$50_0^3 75_0^2$	1104.2	22	$40_0^1 49_0^1$
416.1	11	$73_0^2 74_0^2$	1141.0	4	$40_0^1 48_0^1$
427.5	23	$49_0^1 74_0^2$	1206.8	15	27_0^1
429.5	6	$48_0^1 50_0^1$	1279.0	3	$27_0^1 75_0^2$
444.2	5	74_0^6	1320.2	4	$27_0^1 50_0^1$
459.5	4	73_0^2 (192)	1354.5	4	$27_0^1 74_0^2$
465.8	8	$48_0^1 74_0^2$	1385.2	4	$40_0^1 49_0^2$
471.2	6	2× (236)	1475.5	3	$27_0^1 73_0^2$
481.6	9	47_0^1	1487.1	7	$27_0^1 49_0^1$
494.5	4	$50_0^2 73_0^2$	1530.2	7	$27_0^1 48_0^1$
536.1	6	73_0^4	1648.3	8	40_0^2
542.2	4	$48_0^1 50_0^2$	1767.3	5	$27_0^1 49_0^2$
547.8	15	46_0^1	2030.7	5	$40_0^1 27_0^1$

of the electronic wave function of the lending state, and $\Gamma(Q_t)$ the symmetry species of the induced normal coordinate. Evidently, the calculated symmetry species of the lowest excited electronic states do not support a Herzberg−Teller coupling mechanism, since an excited-state electronic wave function of A'' symmetry would be required to induce a normal mode of a'' symmetry. Moreover, neither the transitions labeled (192), (236), and their combination bands nor those labeled as Fermi resonances are likely to be due to impurities (as, e.g., 1-phenylindene or 3-phenylindene) as can be seen from the excess energy dependence of the fluorescence lifetimes given in Figure 5, unless the fluorescence lifetimes of the alleged impurity accidentally fit in the energy dependence of Figure 5. Unfortunately, no hole-burning experiments could be carried out with our present experimental setups in order to check the presence of other conformers. Nonetheless, it seems very unlikely that these transitions are due to other conformers, since the potential function of the lowest-frequency normal mode of the S_0 state, the torsional normal mode, does not support the assumption of another stable conformer (see Figure 6).

TABLE 6: Experimental Frequencies ν_{FES} of the Fluorescence Excitation Spectrum and Frequencies ν_{calc} Calculated on the CIS/6-31G(d,p) Level of Theory

ν_{FES} [cm^{-1}]	ν_{calc} [cm^{-1}]	$\Gamma_j^{(1)}(l_i')$	S_1 normal mode
33.6	37.3	a″	ν_{75}
76.3	67.5	a″	ν_{74}
113	109	a′	ν_{50}
134	129	a″	ν_{73}
192	194	a″	ν_{72}
236	243	a″	ν_{71}
281	269	a′	ν_{49}
317	309	a′	ν_{48}
482	479	a′	ν_{47}
548	538	a′	ν_{46}
589	595	a′	ν_{44}
754	728	a′	ν_{42}
806	803	a′	ν_{41}
824	850	a′	ν_{40}
1207	1205	a′	ν_{27}

TABLE 7: Symmetry Species and Vertical Excitation Energies VE_{calc} of the Lowest Triplet and Singlet Excited Electronic States Calculated on the CIS/6-31G(d,p) Level of Theory with the B3LYP/6-31G(d,p) Equilibrium Geometry

state	symmetry	VE_{calc} [nm]	VE_{exp} [nm]
S_0	$\tilde{X}\ ^1A'$		
T_1	$\tilde{a}\ ^3A'$	547	
T_2	$\tilde{b}\ ^3A'$	374	
T_3	$\tilde{c}\ ^3A'$	318	
S_1	$\tilde{A}\ ^1A'$	266	318
T_4	$\tilde{d}\ ^3A'$	266	
T_5	$\tilde{e}\ ^3A'$	262	
T_6	$\tilde{f}\ ^3A'$	255	
S_2	$\tilde{B}\ ^1A'$	215	
S_3	$\tilde{C}\ ^1A'$	212	
S_4	$\tilde{D}\ ^1A'$	199	
S_5	$\tilde{E}\ ^1A'$	177	
S_6	$\tilde{F}\ ^1A'$	171	

Third, the intensity discrepancy between the FES spectrum and the REMPI spectrum illustrated in Figure 3 is not understood yet. Perhaps, this is the most interesting and most enigmatic spectroscopic property of 2-phenylindene. To the best of our knowledge, no investigation revealing a similarly strong intensity discrepancy between FES and REMPI spectra has been published so far. It should be pointed out that the vibronic transitions in both spectra are identical; only their relative intensities differ. Particularly, it should be stressed that these intensity differences cannot be attributed to the neglect of corrections for laser power. For example, we measured the FES and REMPI spectra of *trans*-stilbene[35,37] with and without corrections for the laser power curves (which all perfectly reproduced previously reported spectra[74,80−82]) and noticed only minor intensity differences (∼10% of the intensity of each transition). Moreover, comparison of the medium-resolution FES spectrum (Figure 3b) with the low-resolution FES spectrum (Figure 5) gives an indication of the uncertainties concerning relative fluorescence intensities. The FES spectrum of Figure 3b consists of 13 pieces of different lengths (150−550 cm^{-1}) and was measured with two laser dyes: DCM (638−610 nm) and RhodamineB (611−587 nm). The FES spectrum of Figure 5 consists of 7 pieces of different lengths (200−1100 cm^{-1}) and was measured with two laser dyes: SulforhodamineB (640−603 nm) and Rhodamine6G (604−573 nm). From our point of

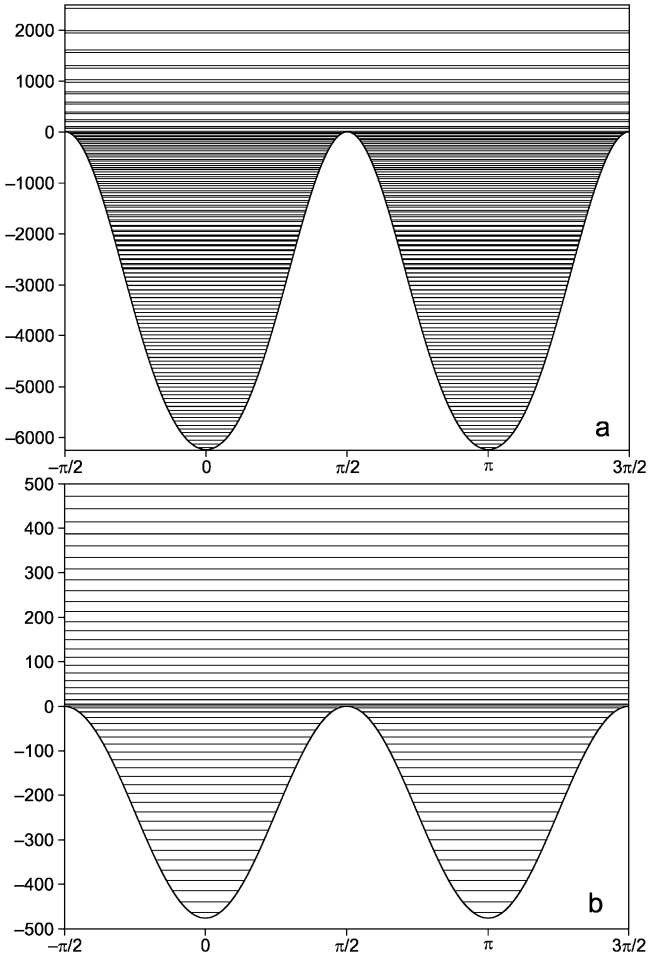

Figure 6. Simulated torsional potentials and torsional energy levels [cm^{-1}] of the S_1 state (a) and the S_0 state (b).

TABLE 8: Calculated Vertical and Adiabatic Ionization Potentials (IP).

basis set	vertical IP [cm^{-1}]	basis set	adiabatic IP [cm^{-1}]
6-31G	54997	6-31G(d)	55033
6-31G(d)	56130	6-311G(d)	56879
6-31G(d,p)	56621	6-311++G(d,p)	57342

view, there are only minor intensity differences due to different dye-laser power curves and different spectral overlap regions of the laser dyes.

In an attempt to account for this intensity anomaly, vertical and adiabatic ionization potentials were calculated (Table 8). For an assessment of the quality of the calculations, the adiabatic ionization potential of *trans*-stilbene was also calculated (IP = 58 350 cm^{-1} with the UB3LYP/6-311+G(d) and B3LYP/6-311+G(d) methods; IP = 58 522 cm^{-1} with the UB3LYP/6-311++G(d,p) and RB3LYP/6-311++G(d,p) methods). The comparison of the calculated values of *trans*-stilbene with the experimentally determined adiabatic ionization potential of IP = 61 748 cm^{-1} [83] shows that the calculated values are ∼5% too low. Thus, an adiabatic ionization potential of IP = (60 000 ± 1000) cm^{-1} can be estimated for 2-phenylindene. Two-photon ionization from the 0_0^0 level (2 × 31 409.4 cm^{-1}) yields an excess energy of the cation of ∼3000 cm^{-1}. Considering that the strongest intensity discrepancies occur only for excess energies of >950 cm^{-1}, which correspond to excess energies of >4900 cm^{-1} in the cation, a strong energy dependence of the ionization cross-section at these excess energies cannot be expected. On our present level of theoretical information, intersystem crossing from the first excited singlet state S_1 to the energetically contiguous manifold of three triplet states T_4, T_5, and T_6 (Table 7) might provide an explanation for the intensity anomaly. Their vertical excitation energies calculated on the CIS/6-31G(d,p) level of theory are 266 nm (T_4), 262 nm (T_5), and 255 nm (T_6). In particular, the triplet state T_4 is energetically close to the first excited singlet state S_1. Interestingly, they are accidentally quasi-degenerate. In the case of intersystem crossing, following excitation of the S_1 state, ionization from the vibronic states of the triplet manifold would be viable, while the fluorescence intensity would be quenched. From our point of view, further theoretical efforts have to be undertaken in order to check our conjecture and to elucidate the intensity anomaly.

TABLE 9: Comparison of the Experimental and Calculated Relative Fluorescence Intensities of the Transitions of Normal-Mode ν_{49} in the Fluorescence Excitation Spectrum

	I_{FES}	I_{calc} $d = 0.145$ Å	I_{opt} $d = 0.165$ Å
0_0^0	1.00	1.00	1.00
49_0^1	0.76	0.59	0.76
	0.36	0.19	0.31
49_0^3	0.15	0.05	0.09

Corroborating evidence in favor of our assignment of the S_1 torsional frequency is furnished by the low-resolution FES spectrum (1.5−3.0 cm^{-1}) recorded under continuous expansion conditions (Figure 5). With the S_0 torsional mode having a frequency of 23 cm^{-1}, the transitions at 51.6 and 331.6 cm^{-1} can directly be assigned to the sequence transitions T_1^1 and 49_0^1 T_1^1, respectively, thus yielding a S_1 torsional frequency of ∼75 cm^{-1}. This value is in good agreement with the calculated value of 67.5 cm^{-1} (CIS/6-31G(d,p)) and with the value of 76.3 cm^{-1} obtained from the cold FES spectrum of Figure 3.

The most prominent progression with a frequency interval of ∼280 cm^{-1} is due to the totally symmetric in-plane stretching mode ν_{49}. The intensity distribution of the overtone transitions of this normal mode can theoretically be reproduced with the help of the ab initio calculations of the S_0 and S_1 states (B3LYP/6−31 g(d,p) and CIS/6-31G(d,p), respectively). The expansion coefficients d_j of the nuclear displacements upon electronic excitation in the basis of the S_1 normal coordinates l'_{ij} were obtained by projecting the difference vector Δr_i of the equilibrium geometries (in Cartesian coordinates) of the S_0 and S_1 states onto the normal coordinates l'_{ij} of the S_1 state

$$\Delta r_i = r'_i - r''_i \quad i = 1, ..., 3N \tag{2}$$

$$\sum_{i=1}^{3N} \Delta r_i l'_{ij} = d_j \quad j = 1, ... 3N - 6 \tag{3}$$

These coefficients d_j were used for the calculation of the fluorescence intensities of the observed overtones according to the procedure of Ansbacher.[84] Harmonic potential functions were assumed for both electronic states

$$V_1 = \frac{1}{2} k_1 q_j^2 \quad V_2 = \frac{1}{2} k_2 (q_j - d_j)^2 \quad j = 1, ..., 3N - 6 \tag{4}$$

where d_j (Å) is the separation of the equilibrium positions of the one-dimensional potentials along the *j*th normal coordinate. Overlap integrals $I(m, n; \beta, \gamma)$ were determined according to eq 3 of ref 84. The intensities of Table 9 were obtained by taking the square of the calculated overlap integrals and by setting the intensity of the 0_0^0 transition arbitrarily to 100. In Table 9, the calculated intensities I_{calc} are compared with the observed

experimental intensities I_{FES} and with optimal intensities I_{opt} obtained by treating the displacement coefficient d as a fit parameter. The comparison of the coefficients d ($d = 0.145$ Å and $d = 0.165$ Å) shows that the ab initio calculations predict a reasonably reliable geometry change upon electronic excitation for normal mode ν_{49}.

Qualitatively, the normal modes ν_{49} and ν_{50} are predicted to have the most prominent fundamentals in the spectrum. The prominent overtone progression of normal mode ν_{40}, however, is strongly underestimated by the calculations. Notwithstanding, on the basis of these results, it can be concluded that the combined ab initio calculations on the B3LYP and CIS levels of theory furnish, by and large, reasonable predictions concerning conformational changes upon electronic excitation.

4.1.2. Torsional Potentials. The torsional potentials of the S_0 and S_1 states were determined by fitting the eigenvalues E_ν of an internal rotation Schrödinger equation

$$H\Psi_\nu = \left[-B\frac{\partial^2}{\partial\phi^2} + V(\phi)\right] \quad \Psi_\nu = E_\nu\Psi_\nu \tag{5}$$

to the experimental frequency values of the dipole-allowed overtones of the torsional normal mode (T_0^2, T_0^4, and T_0^6 from the fluorescence excitation spectrum, T_2^0 and T_4^0 from the fluorescence dispersion spectrum of the 0_0^0 band[8]). The periodic potential function of the internal rotation Hamiltonian was approximated by a truncated Fourier expansion

$$V(\phi) = \frac{1}{2}\sum_{n=1}^{4} V_n[1 - \cos(n\phi)] \tag{6}$$

where, because of the expected twofold torsional barrier, only V_2 and V_4 were taken into account. V_2 corresponds to the energy of the torsional barrier, and V_4 represents the anharmonicity of the torsional potential.

The eigenvalues of the internal rotation Hamiltonian were determined according to the procedure of Laane and coworkers.[85] The internal rotation constant B of eq 5 was assumed to be constant along the torsional coordinate for both the S_0 and S_1 states. The ab initio equilibrium geometries calculated on the B3LYP/6-31G(d,p) and CIS/6-311G(d,p) levels of theory were used to determine the internal rotation constants of the S_0 and S_1 states, respectively. For this purpose, the values of the principal moments of inertia along the *a*-axes of both the phenyl moiety and the indene moiety (I^a_{Ph} and I^a_{Ind}) were separately calculated by diagonalizing their corresponding moments of inertia tensors. The reduced moment of inertia I^a_r of the internal rotation of both moieties about their *a*-axes was calculated as

$$I^a_r = \left[\frac{1}{I^a_{Ph}} + \frac{1}{I^a_{Ind}}\right] \tag{7}$$

Finally, the internal rotation constants of both electronic states were determined according to

$$B = \frac{h}{8\pi^2 c I^a_r} \tag{8}$$

Their values are $B = 0.3169$ cm^{-1} for the S_0 state and $B = 0.3138$ cm^{-1} for the S_1 state. The procedure employed for the calculation of the reduced moments of inertia I^a_r corresponds to the method of Pitzer and Gwinn[86] under the assumption of parallel oriented principal moments of the phenyl and indene moieties relative to the principal moments of 2-phenylindene.

TABLE 10: Comparison of the Experimental and Calculated Relative Energy Differences of the Torsional Transitions: Fluorescence Excitation Spectrum (FES) and Fluorescence Dispersion Spectrum (FDS)

transition	ν_{FES}	ν_{Calc}	transition	ν_{FES}	ν_{FDS} [a]	ν_{Calc}
T_0^2	147.7	147.8	T_2^0	44.9	46	48
T_0^4	296.0	295.9	T_4^0		96	95
T_0^6	444.2	444.2				

[a] From ref 8.

The diagonalization of the $N \times N$ Hamilton matrix, where N denotes the number of cos/sin basis functions, yielded according to

$$\mathbf{C}^{-1}\mathbf{H}'\mathbf{C} = \mathbf{\Lambda} \tag{9}$$

the diagonal matrix $\mathbf{\Lambda}$, which contains the first N energy eigenvalues $\lambda_\nu = E_\nu/B$, and the coefficient matrix $\mathbf{C}$, whose column vectors contain the expansion coefficients $c_{i\nu}$ of the first N eigenfunctions Ψ_ν in the cos/sin−free-rotor basis $\{\psi_i\}$

$$\Psi_\nu = \sum_{i=1}^{N} c_{i\nu}\psi_i \tag{10}$$

The potential parameters V_2 and V_4 of the S_0 and S_1 states were obtained by matching the observed and calculated torsional frequency spacings in a least-squares fitting procedure. For the S_0 state, the V_2 term turned out to be sufficient for a satisfactory match of the torsional frequency spacings. A comparison of the calculated frequency spacings with the frequency spacings of the S_1 state obtained from the fluorescence excitation spectrum and with the frequency spacings of the S_0 state obtained from the fluorescence dispersion spectrum of HBBZ[8] is given in Table 10.

According to the pertinent dipole selection rule for nontotally symmetric a''-vibrations, only overtone transitions with an even number of torsional quanta have nonvanishing intensities. The simulations were carried out with $\{\psi_i\}$-basis sizes up to $N = 200$. Convergence of the calculated torsional energy eigenvalues, however, was already observed at $N = 50$. As can be seen from Table 10, excellent matches were obtained for the S_1 state with $V_2 = 6245$ cm^{-1} and $V_4 = -478$ cm^{-1}, and for the S_0 state with $V_2 = 476$ cm^{-1}. These sets of simulated potential parameters as well as those obtained from fitting ab initio calculations for both electronic states according to the potential eq 6 are tabulated in Table 11 for comparison. The torsional potentials of the S_0 and S_1 states are depicted in Figure 6 together with several torsional energy levels.

As 2-phenylindene possesses deep, symmetric torsional double-minimum potentials in both electronic states, the torsional energy levels at the bottom of the potentials are accidentally doubly degenerate, i.e., the *even* (cos) and *odd* (sin) wave functions belong in pairs to the same eigenvalues.

Relative fluorescence intensities were calculated by approximating the requisite vibrational overlap integrals by discrete scalar products of expansion coefficients $c_{i\nu}$. Absorption intensities, comparable to the intensities of the fluorescence excitation spectrum, were calculated according to

$$I(T_0^n) \propto \left(\sum_{i=1}^{N} c_{i0}^{S_0,\text{even}}\, c_{in}^{S_1,\text{even}}\right)^2 + \left(\sum_{i=1}^{3} c_{i0}^{S_0,\text{odd}}\, c_{in}^{S_1,\text{odd}}\right)^2 \tag{11}$$

TABLE 11: Parameters of the Fits to the ab Initio Calculated Torsional Potentials According to the Torsional Potential Function Eq 6: S_0 State (above) and S_1 State (middle)[a]

method	V_2 [cm^{-1}]	V_4 [cm^{-1}]
HF/6-31G(d,p)	792	−261
B3LYP/6-31G(d,p)	1475	−290
B3PW91/6-31G(d,p)	1408	−292
MPW1PW91/6-31G(d,p)	1418	−295
SVWN/6-31G(d,p)	2253	−341
CIS/6-31G(d,p)	6957	−883
TDDFT/6-31G(d,p) at CIS/6-31G(d,p)-MEP	6708	−737
Simulations		
S_0	476	
S_1	6245	−478

[a] The values of the torsional potential simulations are given below.

TABLE 12: Comparison of the Experimental and Calculated Relative Fluorescence Intensities of the Torsional Transitions from the Fluorescence Excitation Spectrum (FES) and from the Fluorescence Dispersion Spectrum (FDS)

transition	I_{FES}	I_{calc}	transition	I_{FDS} [a]	I_{calc}
0_0^0	100	100	0_0^0	100	100
T_0^2	31	13	T_2^0	17	13
T_0^4	11	3	T_4^0	4	3
T_0^6	5	0.6			

[a] From ref 8.

emission intensities, comparable to the intensities of the fluorescence dispersion spectrum,[8] were calculated according to

$$I(T_n^0) \propto \left(\sum_{i=1}^{N} c_{in}^{S_0,\mathrm{even}}\, c_{i0}^{S_1,\mathrm{even}}\right)^2 + \left(\sum_{i=1}^{N} c_{in}^{S_0,\mathrm{odd}}\, c_{i0}^{S_1,\mathrm{odd}}\right)^2 \quad (12)$$

Account has been taken in both cases of the double degeneracy of the torsional energy levels at the bottom of the torsional potentials. As *even* ↔ *odd* transitions are forbidden in the conventional approximation framework comprising the Born−Oppenheimer and Condon approximations, coherent terms in the summations of eqs 11 and 23 are missing. A comparison of the calculated Franck−Condon factors and the fluorescence intensities of the observed torsional overtones is given in Table 12. The intensity of the 0_0^0 band origin was arbitrarily set to 100. While the calculated Franck−Condon factors show good agreement with the FDS intensities, the poor agreement with the FES intensities should be noted. Two explanations seem plausible for this discrepancy.

First, FDS intensities seem more likely to be adequately reproduced by eq 12 than FES intensities by eq 11. This expectation rests upon the simple fact that the intensity of an FDS band derives from the fluorescence of a single vibronic transition, whereas the intensity of an FES band is made up of the fluorescence of many vibronic transitions originating in a distinct vibrational level of the excited-state S_1 and terminating in the vibrational manifold of the ground-state S_0. For the calculation of FES Franck−Condon factors, therefore, it seems more appropriate to invoke the quantum-mechanical sum rule[87,88]

$$\sum_i |\mathbf{R}_{gi,kj}|^2 = \int \phi_j^k(Q)\, \mathbf{R}_{g,k}^2(Q)\, \phi_j^k(Q)\, \mathrm{d}Q \quad (13)$$

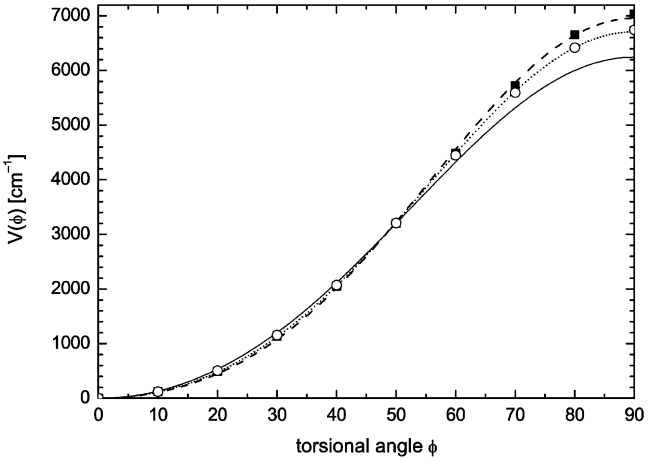

Figure 7. Ab initio calculated torsional potentials and simulated torsional potential of the S_1 state: full line, simulation; ■ and dashed line, CIS/6-31G(d,p); ○ and dotted line, TDDFT/6-31G(d,p) energy calculations on the CIS/6-31G(d,p)−MEP geometries.

which accommodates vibronic transitions terminating in a manifold of vibrational levels, but which, on the other hand, is difficult to evaluate numerically because of the unknown dependence of the electronic transition moment $\mathbf{R}_{g,k}(Q)$ on the set of normal coordinates Q. Second, the poor agreement between the calculated Franck−Condon factors and the FES intensities could be linked to the intensity anomaly between the FES and REMPI spectrum. As a similar anomaly is not documented in the literature, we can only speculate about it having an influence on the aforementioned discrepancy.

In conclusion, the good agreement between the simulated S_1 torsional potential and the ab initio potential calculated on the CIS/6-31G(d,p) level of theory should be stressed. As can be seen from Figure 7, the inclusion of dynamic electron correlation via TDDFT energy calculations on the CIS/6-31G(d,p)−MEP geometries slightly improves the match between the calculated and ab initio S_1 potentials. Both ab initio potentials show good agreement with the simulated potential with regard to the energy barrier ($V_2 = 6957$ cm^{-1} for CIS/6-31G(d,p), $V_2 = 6708$ cm^{-1} for TDDFT/6-31G(d,p)//CIS/6-31G(d,p), and $V_2 = 6245$ cm^{-1} for the simulation) as well as with regard to the sign and degree of anharmonicity ($V_4 = -883$ cm^{-1} for CIS/6-31G(d,p,), $V_4 = -737$ cm^{-1} for TDDFT/6-31G(d,p)//CIS/6-31G(d,p), and $V_4 = -478$ cm^{-1} for the simulation). From our findings, it can, thus, certainly be concluded that the CIS method provides a reliable S_1 torsional potential for the phenyl ring twist in 2-phenylindene.

To the best of our knowledge, so far only the publication by Egawa and co-workers[10] on the symmetric Ph−O torsion in phenyl acetate dealt with the spectroscopic assessment of a torsional potential calculated with the CIS method. Exactly in the fashion of our present contribution, they compared their calculated potential function with a torsional potential obtained by matching the observed Ph−O torsional spacings to simulated spacings. In accordance with our findings for 2-phenylindene concerning the S_1 geometry, normal-mode frequencies, and torsional potential calculated on the CIS level, they obtained very good values for the low-frequency torsional normal modes (Ph−O torsion and CO−O torsion) and a Ph−O torsional potential function in close agreement to the simulated function. We, therefore, feel confident that the CIS method will prove to yield reliable descriptions of the torsion about single bonds in the S_1 states of other nonrigid molecules.

As to the S_0 torsional potential, the comparison of the potential parameter $V_2 = 476$ cm^{-1} obtained from the torsional

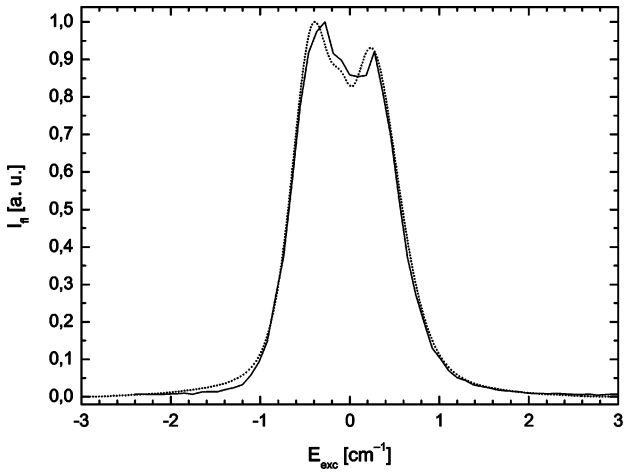

Figure 8. Rotational band contour of the 0_0^0 transition of the REMPI spectrum (full line) and rotational band contour simulation (dotted line). The rotational temperature is $T_{rot} = 7$ K.

potential simulation with those determined from the HF and different DFT calculations (Table 11) reveals strong discrepancies. The ab initio calculations predict torsional barriers which are higher in energy by a factor of 2−4 and a non-negligible anharmonicity. Only the torsional potential calculated on the MP2/6-31G level of theory yields an acceptable torsional barrier of ∼450 cm^{-1}. As has already been discussed in section 4.1.1, the equilibrium geometries of 2-phenylindene calculated with the MP2 method, however, do not possess mirror symmetry ($\phi \neq 0$). With the MP2/6-31G method, the equilibrium geometry is predicted to have a torsional angle ϕ of 34°. Therefore, it was not possible to fit the MP2 potential analytically according to eq 6.

In addition to the calculation of torsional potentials, transition-state geometries were located in both electronic states using the synchronous transit-guided quasi-Newton method (STQN).[57,58] The transition-state search was performed on the B3LYP/6-31G-(d) level of theory for the S_0 state and on the CIS/6-31G(d) level of theory for the S_1 state. In Figure 2, the transition-state conformation of the excited state is depicted. The torsional angle $\phi = \angle(7, 8, 15, 16)$ has a value of −90.5°. The single imaginary frequency corresponding to the torsional motion of the phenyl ring around the indene moiety has a value of i96.1 cm^{-1} (unscaled). The corresponding values of the S_0 state are −90.4° and i55.2 cm^{-1} (unscaled). The S_0 transition-state geometry, however, does not show the ring-puckering type of deformation, which is clearly discernible in Figure 2 for the S_1 geometry. The calculation of the energy difference between the S_1 equilibrium geometry and the S_1 transition-state geometry yielded a torsional barrier of $E_0 = 6745$ cm^{-1} in the excited state. Thus, the potential parameter $V_2 = 6957$ cm^{-1} of the CIS/6-31G(d,p) potential function is confirmed to correspond to the energy of the torsional barrier. As to the ground state, a torsional barrier of $E_0 = 1399$ cm^{-1} was calculated on the B3LYP/6-31G(d) level of theory, which corroborates the unfavorable result already obtained from the B3LYP/6-31G(d,p) torsional potential calculation.

4.1.3. Rotational Band Contour. The rotational band contour of the vibrationless electronic transition 0_0^0 was experimentally determined with the same REMPI setup which has already been used for the measurement of the REMPI spectrum. Figure 8 shows the experimental band contour together with a fit which was obtained with the freeware program PGOPHER.[89] Fit parameters were the rotational constants of both electronic states, the rotational temperature T_{rot}, and the full widths at half-maxima (fwhm) of a Gaussian and a Lorentzian line profile constituting in total a Voigt profile. The best fit was obtained by varying single parameters manually and inspecting visually every change. The following estimates for the uncertainties of the fit parameters were determined by visual inspection of the P−R-branch separation, the P−R-branch intensity ratio and the relative Q-branch intensity: $\Delta A = \pm 0.0120$ GHz, $\Delta B = \Delta C = \pm 0.0020$ GHz, $\Delta T = \pm 1$ K, and Δfwhm $= \pm 0.05$ cm^{-1}. It should be borne in mind, however, that the set of fit parameters determined from the simulation of the rotational band contour is certainly not unique and, therefore, it is preferable to consider only the sums $B + C$ as reliable. Selection rules appropriate for long-axis (parallel) polarization of the $S_1 \leftarrow S_0$ transition dipole moment were assumed. The rotational constants of the S_0 and S_1 states yielding the best fit to the experimental rotational contour are given in Table 4 together with the ab initio calculated rotational constants for comparison. The best-fit sum $B + C = 0.5485$ GHz of the S_1 state is in good agreement with the calculated sum $B + C = 0.5459$ GHz obtained from the CIS/6-31G(d,p) calculation. It also agrees well with the sum $B + C = (0.5499 \pm 0.077)$ GHz obtained from the analysis of the time-domain fluorescence measurements (see section 4.2.2). For both electronic states, the calculated rotational constants B and C show good agreement with those obtained from the analysis of the rotational contour. However, the calculated rotational constants A deviate strongly from those obtained experimentally. The calculated value of the ground electronic state is 0.0540 GHz higher than its experimental counterpart, the calculated value of the excited electronic state 0.0374 GHz.

The best rotational contour fit shown in Figure 8 furnished a rotational temperature of $T_{rot} = 7$ K, which is in good agreement with the value of $T_{rot} = 10$ K obtained from the analysis of the time-domain fluorescence measurements (see section 4.2.2). The simulated rotational line structure had to be convoluted with the product of a Gaussian line shape (fwhm $= 0.15$ cm^{-1}) and a Lorentzian line shape (fwhm $= 0.22$ cm^{-1}). The fwhm of the Gaussian line shape agrees well with the temporal laser pulse width of $\Delta\tilde{\nu} \leq 0.15$ cm^{-1}. No account has been taken of the strong asymmetry of the temporal laser pulse profile.

In summarizing the information obtained from the fit of the rotational band contour, it should be pointed that the ab initio calculations for both the ground and excited states furnished, by and large, rotational constants in close agreement to the experimental values determined from the frequency-domain rotational contour measurement.

4.2. Dynamics. *4.2.1. Fluorescence Lifetimes.* The fluorescence lifetimes $\tau_{fl}(E)$ of jet-cooled isolated 2-phenylindene were determined as a function of excess vibrational energy. The fluorescence decay curves were analyzed by a least-squares convolution and fitting routine using the Levenberg−Marquardt algorithm.[90,91] As an example, in Figure 9, the fluorescence decay curve at $E_{exc} = 3291$ cm^{-1} is given together with a single-exponential fit. The residuals and their autocorrelation function (ACF) illustrate the high quality of the fit. All fluorescence decay curves could be fitted satisfactorily by single-exponential functions.

This finding is in agreement with the results of Heikal, Baskin, Bañares, and Zewail[8] as well with the findings of Dutt, Konitsky, and Waldeck.[33] The former reported single-exponential fits over the entire excess energy range 0−5500 cm^{-1} studied under supersonic jet conditions, and the latter single-exponential fits to the fluorescence decay curves measured in different alkane solvents, methanol and acetonitrile.

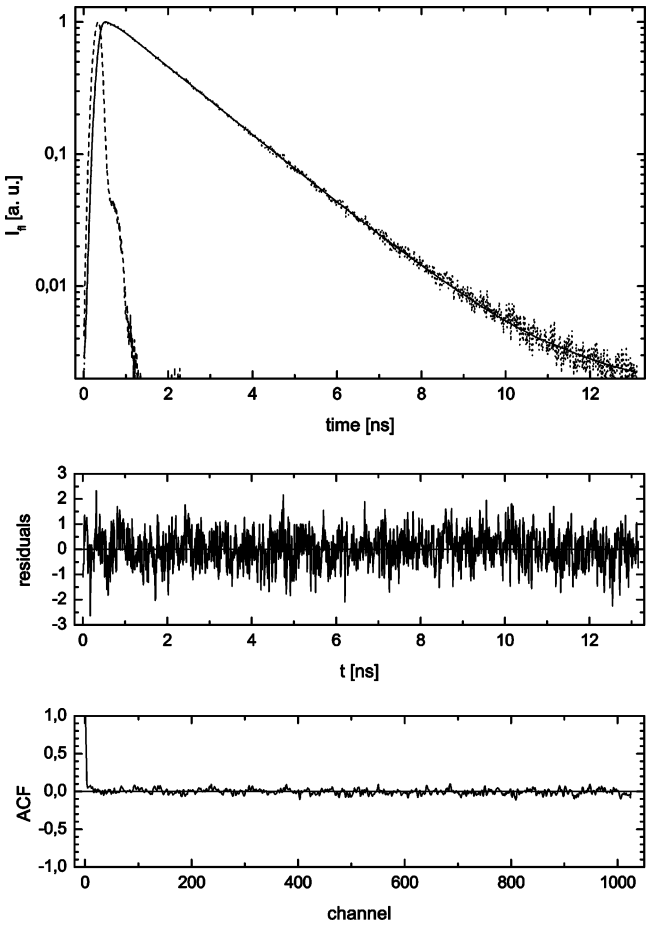

Figure 9. Fluorescence decay curve at $E_{exc} = 3291$ cm^{-1} with monoexponential fit $\tau_{fl} = 1.670$ ns.

Specific rate constants $k(E)$ of the nonradiative intramolecular process were calculated according to

$$k(E) = \frac{1}{\tau_{fl}(E)} - k_{rad} \tag{14}$$

where k_{rad} denotes the rate constant of the radiative process, which was assumed to be excess energy independent. Its value $k_{rad} = 3.08 \cdot 10^8$ s^{-1} was calculated as the arithmetic mean of the fluorescence lifetimes in the excess energy range 0−850 cm^{-1}. Our specific rate constants $k(E)$ show very good agreement with those of HBBZ[8] in the excess energy range we have studied.

The filled circles in Figure 5 indicate the fluorescence lifetimes of hot bands involving the torsional normal mode (T_1^1 at 51.6 cm^{-1} and $49_0^1T_1^1$ at 331.6 cm^{-1}), which appear only under continuous expansion conditions.

As is clearly discernible from Figure 5, the energy dependence of the fluorescence lifetimes signals the onset of an intramolecular radiationless process around 1600 cm^{-1}. However, as the simulated and the ab initio calculated potential barriers of the internal rotation clearly suggest, this intramolecular process cannot be attributed to the torsion of the phenyl ring against the indene moiety. Particularly, the energy barrier of $E_0 = (1770 \pm 70)$ cm^{-1} obtained from a nonadiabatic RRKM fit of the specific rate constants $k(E)$ by HBBZ[8] cannot be interpreted as a torsional barrier.

Finally, it should be noted that neither the attempt to fit the energy dependence of the specific rate constants $k(E)$ by a conventional RRKM fit using the S_1 equilibrium and transition-state frequencies of Table 7 and varying the barrier energy E_0 in the standard RRKM expression

$$k(E) = \frac{W^{\ddagger}(E - E_0)}{h \cdot \rho(E)} \tag{15}$$

nor the attempt to fit the specific rate constants according to Fermi's Golden Rule

$$\frac{1}{\tau_{fl}(E)} = k_{fl}(E) = k_{rad} + \frac{2\pi}{\hbar}|V_{if}|^2 \rho_{S_0}(E)$$
$$= k_{rad} + c \cdot \rho_{S_0}(E) \tag{16}$$

using the S_0 equilibrium frequencies and varying the parameter c yielded satisfactory outcomes.

Furthermore, we feel reluctant to link the uniform energy dependence of the fluorescence lifetimes depicted in Figure 5 to the potential barrier of a so-called phototransposition reaction. Phototransposition reactions were observed in solution with different mono-, di-, and trisubstituted indenes and were interpreted mechanistically in two different ways.[92−96] Both explanations comprise pericyclic steps of different types, but lead through a common intermediate containing a three-membered ring. The hypothetical phototransposition reaction of 2-phenylindene would lead to 1-phenylindene and 3-phenylindene. It does not seem probable, however, that the hypothetical intermediate containing the three-membered ring is energetically more favorable than the simple, sterically unstrained transition state of the internal rotation. In particular, from chemical intuition, this type of intermediate is unlikely to be reached through a transition state of as low an energy barrier as $E_0 \approx 1600$ cm^{-1}. On our present level of theoretical information, the apparent onset of an intramolecular radiationless process could be explained by the occurrence of intersystem crossing from the first excited singlet state S_1 to the energetically contiguous manifold of three triplet states T_4, T_5, and T_6 (see Table 7), as already invoked in the explanation of the intensity anomaly of section 4.1.1. It should be noted, however, that the attempt to fit the specific rate constants according to Fermi's Golden Rule eq 16 using ab initio T_4 normal-mode frequencies and treating c as a free parameter did not yield satisfactory results. Thus, from our point of view, a quantitative understanding of the uniform energy dependence of the fluorescence lifetimes depicted in Figure 5 is worth of further investigation.

4.2.2. Rotational Coherence Spectroscopy. The transients of fluorescence anisotropy decay curves measured under supersonic jet conditions with narrow spectral bandwidth excitation are a manifestation of purely rotational coherence.[97−101] Rotational coherence spectroscopy has proven to be a valuable means to obtain sub-Doppler information, i.e., rotational constants of excited electronic states, on large molecules and clusters in the time domain, even when the resolution in the frequency domain is Doppler-limited.

In Figure 10a, rotational coherence signals of 2-phenylindene with parallel and perpendicular detection polarizations are given together with simulations.

The simulations were carried out according to a Fourier expansion, eq 2.2 of ref 98. As the absorption dipole moment direction was determined to be parallel according to the CIS calculations (see section 4.1.1), ||, || dipole directions were assumed for the calculation of the rotational coherence recurrences. Thus, the Fourier amplitudes $f_i(J_0, K_0, \hat{\mathbf{e}}_{fl})$ and their corresponding frequencies ν_i were calculated according to Table 1 of ref 98. The rotational constant B of the symmetric prolate

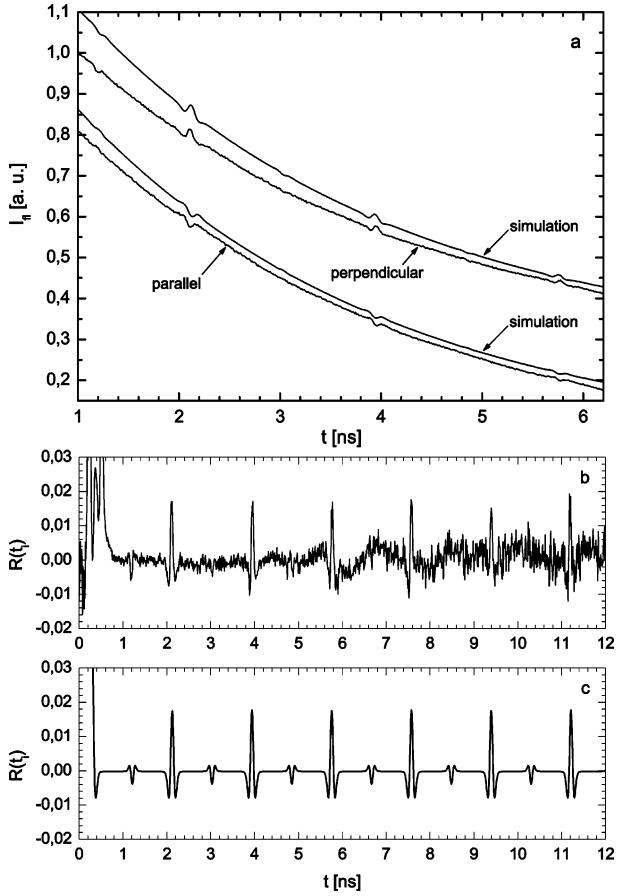

Figure 10. Rotational coherence signals at parallel and perpendicular detection polarizations together with simulations (a): $T_{rot} = 10$ K, $\tau = 3.072$ ns. The simulated curves were convoluted with an instrument response function of Gaussian shape (fwhm = 85 ps). Experimental (b) and calculated (c) anisotropy signals $R(t_i)$ were formed from the above decay curves.

top was replaced by the approximate rotational constant $\tilde{B} = 0.5(B + C)$ of the slightly asymmetric prolate top.

The sum of the S_1 rotational constants $B + C = (0.5499 \pm 0.0077)$ GHz used for the simulations was obtained from an analysis of the anisotropy[99]

$$R(t_i) = \frac{I_{||}(t_i) - I_{\perp}(t_i + \beta)}{I_{||}(t_i) + 2 \cdot I_{\perp}(t_i + \beta)} \tag{17}$$

$I_{||}(t_i)$ and $I_{\perp}(t_i)$ are the intensities in the ith channel of the fluorescence decay curves measured with parallel and perpendicular detection polarizations, respectively. β is an adjustable parameter with which $I_{\perp}(t_i)$ was shifted relative to $I_{||}(t_i)$ in order to obtain as many as possible symmetrical anisotropy transients. The necessity to consider the parameter β is engendered by the unavoidable change of the fluorescence path concomitant with the change of the detection polarization.

The recurrence time $\Delta t = (1.819 \pm 0.026)$ ns of the anisotropy transients was calculated as the arithmetic mean of the time spacings of the six maxima given in Figure 10b. The sum of the S_1 rotational constants $B + C$ was determined according to

$$\Delta t = \frac{1}{B + C} \tag{18}$$

As to all other rotational constants needed for the simulations of Figure 10, their ab initio calculated values given in Table 4 were used. The maximal rotational quantum numbers J_0^{max} and K_0^{max} were set to 50. Simulations with maximal rotational quantum numbers up to $J_0^{max} = K_0^{max} = 200$ were carried out in order to make sure that no changes occur from the simulations with $J_0^{max} = K_0^{max} = 50$.

For the comparison with the experimental RCS signals, the simulated transients were multiplied with a single-exponential decay curve ($\tau = 3.072$ ns) and convoluted with an instrument response function of Gaussian shape, whose full width at half-maximum corresponds to the experimentally determined value (fwhm = 85 ps). Unfortunately, the experimentally determined RCS signals are superposed by an intense artifact of unknown origin at early delay times, which prevented an automatic least-squares fit. Therefore, the impact of changes of the free fit parameters T_{rot} and τ on the quality of the fit were merely assessed by visual inspection. The deviation of the time constant $\tau = 3.072$ ns used in the simulations from the experimentally determined fluorescence lifetime $\tau_{fl} = 3.268$ ns of the 0_0^0 transition is, certainly, due to the distortion of the decay curve caused by the artifact. The simulations yielded a rotational temperature of $T_{rot} = (10 \pm 2)$ K, which is in good agreement to the value of $T_{rot} = 7$ K obtained from the simulation of the 0_0^0 rotational band contour (see section 4.1.3).

Concluding this section, we would like to stress the good agreement between the sum of the S_1 rotational constants $B + C$ determined from the analysis of the RCS signals with their ab initio values calculated on the CIS level of theory. The value of $B + C = 0.5575$ GHz calculated on the CIS/6-31G(d,p) level of theory under the restriction of C_s point group symmetry lies within the error of the experimental value $B + C = (0.5499 \pm 0.0077)$ GHz. Furthermore, the simulation of the RCS signals provides additional evidence for a parallel $S_1 \leftarrow S_0$ transition dipole moment as predicted on the CIS level of theory.

5. Conclusion

We investigated the spectroscopy of the first excited electronic state S_1 of 2-phenylindene using both fluorescence excitation spectroscopy and resonantly enhanced multiphoton ionization spectroscopy. Moreover, we investigated the dynamics of the S_1 state by determining state-selective fluorescence lifetimes up to an excess energy of $\sim$3400 cm^{-1}.

In an effort to assess the appropriateness of ab initio calculations carried out on the CIS level of theory to account for our spectroscopic and dynamic findings, we performed S_1-state calculations of the torsional potential energy curve and the equilibrium and transition-state geometries and normal-mode frequencies. Supported by the ab initio calculations, numerous vibronic transitions of the FES and REMPI spectra were assigned, especially those involving the torsional normal mode. The torsional potentials of the ground and first excited electronic states were obtained by matching the observed and calculated torsional frequency spacings in a least-squares fitting procedure. The simulated S_1 potential showed very good agreement with the ab initio potential calculated on the CIS/6-31G(d,p) level of theory. TDDFT energy corrections improved the match with the simulated S_1 torsional potential. The latter calculation yielded a torsional barrier of $V_2 = 6708$ cm^{-1}, and the simulation a barrier of $V_2 = 6245$ cm^{-1}.

As to the ground electronic state, only the MP2/6-31G calculation yielded a torsional barrier of $\sim$460 cm^{-1}, which is in reasonable agreement with the barrier of 476 cm^{-1} obtained from the torsional potential simulation. Ground-state normal-mode frequencies were calculated on the B3LYP/6-31G(d,p) level of theory. They were used to interpret the infrared

spectrum, the FDS spectrum of the 0_0^0 transition,[8] and hot bands of the FES spectrum.

The fluorescence intensities of the ν_{49} overtone progression could reasonably be reproduced by considering the geometry changes upon electronic excitation predicted by the ab initio calculations.

On the basis of the torsional potential calculations, it could be ruled that the uniform excess energy dependence of the fluorescence lifetimes is linked to the torsional barrier in the excited state. The energy dependence of the fluorescence lifetimes showed an onset of a radiationless intramolecular process around 1600 cm^{-1}. On the basis of our excited singlet- and triplet-state calculations, it was suggested that the uniform excess energy dependence of the fluorescence lifetimes could be due to $S_1 \rightarrow T_x$ intersystem crossing with the triplet state T_4 being accidentally quasi-degenerate with the S_1 state and with the triplet states T_5 and T_6 being energetically contiguous. The nature of this process, however, remains unclear, as a quantitative understanding of the energy dependence of the fluorescence lifetimes could not be attained.

The rotational band contour simulation of the 0_0^0 transition yielded rotational constants in close agreement to the ab initio values for both electronic states.

Rotational coherence signals were obtained by polarization-analyzed, time-resolved measurements of the fluorescence decay of the 0_0^0 transition. The simulation of these signals yielded corroborating evidence as to the quality of the ab initio calculated rotational constants of both states.

Moreover, both the simulation of the 0_0^0 rotational band contour and the analysis of the RCS signals yield corroborating evidence in favor of a parallel $S_1 \leftarrow S_0$ transition dipole moment as predicted on the CIS level of theory.

The most puzzling outcome of our work, the intensity discrepancy between the FES spectrum and the REMPI spectrum, could not be accommodated for conclusively. On the basis of our excited singlet- and triplet-state calculations, it was conjectured that the $S_1 \rightarrow T_x$ intersystem crossing could account for this phenomenon as well as for the uniform excess energy dependence of the fluorescence lifetimes. From our point of view, this anomaly is worthy of further theoretical investigation.

Acknowledgment. We would like to thank Dr. K. Wack for performing the rotational coherence measurements. Financial support by the Deutsche Forschungsgemeinschaft (Sonderforschungsbereich 357: Molekulare Mechanismen Unimolekularer Prozesse) is gratefully acknowledged.

Supporting Information Available: Detailed information (8 tables and 1 figure) about the experimental findings and the ab initio calculations reported in our paper: the fluorescence lifetimes, the specific rate constants of the nonradiative intramolecular process, the equilibrium geometry and transition state-geometry of the ground electronic state, the equilibrium geometry and transition-state geometry of the first excited singlet state, the normal-mode frequencies of all four geometries, and the assignment of the infrared spectrum. This material is available free of charge via the Internet at http://pubs.acs.org.

References and Notes

(1) Hollas, J. M.; Ridley, T. *Chem. Phys. Lett.* **1980**, *75*, 94.
(2) Okuyama, K.; Hasegawa, T.; Ito, M.; Mikami, N. *J. Phys. Chem.* **1984**, *88*, 1711.
(3) Werst, D. W.; Gentry, W. R.; Barbara, P. F. *J. Phys. Chem.* **1985**, *89*, 729.
(4) Werst, D. W.; Londo, W. F.; Smith, J. L.; Barbara, P. F. *Chem. Phys. Lett.* **1985**, *118*, 367.
(5) Yamasaki, K.; Arita, K.; Kajimoto, O. *Chem. Phys. Lett.* **1986**, *123*, 277.
(6) Hollas, J. M. *Anal. Proc.* **1991**, *28*, 411.
(7) Monte, C.; Roggan, A.; Subaric-Leitis, A.; Rettig, W.; Zimmermann, P. *J. Chem. Phys.* **1993**, *98*, 2580.
(8) Heikal, A. A.; Baskin, J. S.; Bañares, L.; Zewail, A. H. *J. Phys. Chem. A* **1997**, *101*, 572.
(9) Sinclair, W. E.; Yu, H.; Phillips, D.; Hollas, J. M. *J. Chem. Phys.* **1997**, *106*, 5797.
(10) Egawa, T.; Yamada, T.; Konaka, S. *Chem. Phys. Lett.* **2000**, *324*, 260.
(11) Bock, C. W.; Trachtmann, M.; George, P. J. *Chem. Phys.* **1985**, *93*, 431.
(12) Schaefer, T.; Penner, G. H. *Chem. Phys. Lett.* **1985**, *114*, 526.
(13) Tsuzuki, S.; Tanabe, K.; Osawa, E. *J. Phys. Chem.* **1990**, *94*, 6175.
(14) Head-Gordon, M.; Pople, J. A. *J. Phys. Chem.* **1993**, *97*, 1147.
(15) Setokuchi, O.; Sato, M.; Matuzawa, S.; Simizu, Y. *J. Mol. Struct.* **1996**, *365*, 29.
(16) Förner, W.; Badawi, H. M. *J. Mol. Struct.* **1998**, *454*, 41.
(17) Tsuzuki, S.; Uchimaru, T.; Matsumura, K.; Mikami, M.; Tanabe, K. *J. Chem. Phys.* **1999**, *110*, 2858.
(18) Arulmozhiraja, S.; Selvin, P. C.; Fujii, T. *J. Phys. Chem. A* **2002**, *106*, 1765.
(19) Sakata, K.; Hara, K. *Chem. Phys. Lett.* **2003**, *371*, 164.
(20) Hollas, J. M. *J. Chem. Soc., Faraday Trans.* **1998**, *94*, 1527.
(21) Hargitai, R.; Szalay, P. G.; Pongor, G.; Fogarasi, G. *J. Mol. Struct.* **1994**, *304*, 293.
(22) Choi, C. H.; Kertesz, M. *J. Phys. Chem. A* **1997**, *101*, 3823.
(23) Karpfen, A.; Choi, C. H.; Kertesz, M. *J. Phys. Chem. A* **1997**, *101*, 7426.
(24) Im, H. S.; Bernstein, E. R.; Secor, H. V.; Seeman, J. I. *J. Am. Chem. Soc.* **1991**, *113*, 4422.
(25) Im, H.-S.; Bernstein, E. R. *J. Chem. Phys.* **1988**, *88*, 7337.
(26) Takei, Y.; Yamaguchi, T.; Osamura, Y.; Fuke, K.; Kaya, K. *J. Phys. Chem.* **1988**, *92*, 577.
(27) Barone, V.; Cristinziano, P. *Chem. Phys. Lett.* **1993**, *215*, 40.
(28) Bendazzoli, G. L.; Orlandi, G.; Palmieri, P.; Poggi, G. *J. Am. Chem. Soc.* **1978**, *100*, 392.
(29) Hemley, R. J.; Dinur, U.; Vaida, V.; Karplus, M. *J. Am. Chem. Soc.* **1985**, *107*, 836.
(30) Zilberg, S.; Haas, Y. *J. Chem. Phys.* **1995**, *103*, 20.
(31) Bañares, L.; Heikal, A. A.; Zewail, A. H. *J. Phys. Chem.* **1992**, *96*, 4127.
(32) Qian, J.; Schultz, S. L.; Jean, J. M. *Chem. Phys. Lett.* **1995**, *233*, 9.
(33) Dutt, G. B.; Konitsky, W.; Waldeck, D. H. *Chem. Phys. Lett.* **1995**, *245*, 437.
(34) Daum, R.; Druzhinin, S.; Ernst, D.; Rupp, L.; Schroeder, J.; Zachariasse, K. A. *Chem. Phys. Lett.* **2001**, *341*, 272.
(35) Müller, Ch. Ph.D. Thesis, Georg-August-Universität, Göttingen, 2005 (available at: http://webdoc.sub.gwdg.de/diss/2005/mueller_christian/mueller_christian.pdf).
(36) O'Connor, D. V.; Phillips, D. *Time-correlated Single Photon Counting*; Academic Press: London, 1984.
(37) Klöppel-Riech, M. Ph.D. Thesis, Georg-August-Universität, Göttingen, 2000.
(38) Schröder, F. Ph.D. Thesis, Georg-August-Universität, Göttingen, 2005.
(39) Wiley, W. C.; McLaren, I. H. *Rev. Sci. Instrum.* **1955**, *26*, 1150.
(40) Frisch, M. J.; Trucks, G. W.; Schlegel, H. B.; Scuseria, G. E.; Robb, M. A.; Cheeseman, J. R.; Zakrzewski, V. G.; Montgomery, J. A., Jr.; Stratmann, R. E.; Burant, J. C.; Dapprich, S.; Millam, J. M.; Daniels, A. D.; Kudin, K. N.; Strain, M. C.; Farkas, O.; Tomasi, J.; Barone, V.; Cossi, M.; Cammi, R.; Mennucci, B.; Pomelli, C.; Adamo, C.; Clifford, S.; Ochterski, J.; Petersson, G. A.; Ayala, P. Y.; Cui, Q.; Morokuma, K.; Malick, D. K.; Rabuck, A. D.; Raghavachari, K.; Foresman, J. B.; Cioslowski, J.; Ortiz, J. V.; Stefanov, B. B.; Liu, G.; Liashenko, A.; Piskorz, P.; Komaromi, I.; Gomperts, R.; Martin, R. L.; Fox, D. J.; Keith, T.; Al-Laham, M. A.; Peng, C. Y.; Nanayakkara, A.; Gonzalez, C.; Challacombe, M.; Gill, P. M. W.; Johnson, B. G.; Chen, W.; Wong, M. W.; Andres, J. L.; Head-Gordon, M.; Replogle, E. S.; Pople, J. A. *Gaussian 98*, revision A.7; Gaussian, Inc.: Pittsburgh, PA, 1998.
(41) Foresman, J. B.; Frisch, Æ. *Exploring Chemistry with Electronic Structure Methods*; Gaussian, Inc.: Pittsburgh, PA, 1996.
(42) Wong, M. W. *Chem. Phys. Lett.* **1996**, *256*, 391.
(43) Scott, A. P.; Radom, L. *J. Phys. Chem.* **1996**, *100*, 16502.
(44) Grunenberg, J.; Herges, R. *J. Comput. Chem.* **1997**, *18*, 2050.
(45) Palafox, M. A. *J. Phys. Chem. A* **1999**, *103*, 11366.
(46) Palafox, M. A. *Int. J. Quantum Chem.* **1999**, *77*, 661.
(47) Palafox, M. A.; Gill, M.; Nunez, N. J.; Rastogi, V. K.; Mittal, L.; Sharma, R. *Int. J. Quantum Chem.* **2005**, *103*, 394.

(48) Pople, J. A.; Scott, A. P.; Wong, M. W.; Radom, L. *Isr. J. Chem.* **1993**, *33*, 345.
(49) El-Azhary, A. A.; Suter, H. U. *J. Phys. Chem.* **1996**, *100*, 15056.
(50) Sinha, P.; Boesch, S. E.; Gu, C.; Wheeler, R. A.; Wilson, A. K. *J. Phys. Chem. A* **2004**, *108*, 9213.
(51) Irikura, K. K.; Johnson, R. D., III; Kacker, R. N. *J. Phys. Chem. A* **2005**, *109*, 8430.
(52) Yoshida, H.; Ehara, A.; Matsura, H. *Chem. Phys. Lett.* **2000**, *325*, 477.
(53) Berezin, K. V.; Nechaev, V. V.; Krivokhizhina, T. V. *Opt. Spectrosc.* **2003**, *94*, 398.
(54) Andersson, M. P.; Uvdal, P. *J. Phys. Chem. A* **2005**, *109*, 2937.
(55) Mulliken, R. S. *J. Chem. Phys.* **1955**, *23*, 1997.
(56) Herzberg, G. *Molecular Spectra and Molecular Structure*; Van Nostrand-Reinhold: New York, 1966; Vol. III.
(57) Peng, C.; Schlegel, H. B. *Isr. J. Chem.* **1994**, *33*, 449.
(58) Peng, C.; Ayala, P. Y.; Schlegel, H. B.; Frisch, M. J. *J. Comput. Chem.* **1996**, *17*, 49.
(59) Cederbaum, L. S. *J. Phys. B* **1975**, *8*, 290.
(60) von Niessen, W.; Schirmer, J.; Cederbaum, L. S. *Comput. Phys. Rep.* **1984**, *1*, 57.
(61) Ortiz, J. V. *J. Chem. Phys.* **1988**, *89*, 6348.
(62) Ortiz, J. V. *Int. J. Quantum Chem., Quantum Chem. Symp.* **1988**, *22*, 431.
(63) Ortiz, J. V. *Int. J. Quantum Chem., Quantum Chem. Symp.* **1989**, *23*, 321.
(64) Zakrzewski, V. G.; von Niessen, W. *J. Comput. Chem.* **1993**, *14*, 13.
(65) Lhost, O.; Brédas, J. L. *J. Chem. Phys.* **1992**, *96*, 5279.
(66) Arenas, J. F.; Tocón, I. L.; Otero, J. C.; Marcos, J. I. *J. Phys. Chem.* **1995**, *99*, 11392.
(67) Baranović, G.; Meić, Z.; Maulitz, A. H. *Spectrochim. Acta, Part A* **1998**, *54*, 1017.
(68) Negri, F.; Orlandi, G. *J. Raman Spectrosc.* **1998**, *29*, 501.
(69) Traetteberg, M.; Frantsen, E. B.; Mijlhoff, F. C.; Hoekstra, A. *Acta Crystallogr., Sect. B* **1975**, *31*, 2813.
(70) Hoekstra, A.; Meertens, P.; Vos, A. *Acta Crystallogr., Sect. B* **1975**, *31*, 2813.
(71) Spangler, L. H.; van Zee, R. D.; Blankespoor, S. C.; Zwier, T. S. *J. Phys. Chem.* **1987**, *91*, 6077.
(72) Champagne, B. B.; Pfanstiel, J. F.; Plusquellic, D. W.; Pratt, D. F.; van Herpen, W. M.; Meerts, W. L. *J. Phys. Chem.* **1990**, *94*, 6.
(73) Syage, J. A.; Al Adel, F.; Zewail, A. H. *Chem. Phys. Lett.* **1983**, *103*, 15.
(74) Spangler, L. H.; van Zee, R.; Zwier, T. S. *J. Phys. Chem.* **1987**, *91*, 2782.
(75) Hollas, J. M.; Musa, H.; Ridley, T.; Turner, P. H.; Weisenberger, K. H.; Fawcett, V. *J. Mol. Spectrosc.* **1982**, *94*, 437.
(76) Schroeder, J.; Steinel, T.; Troe, J. *J. Phys. Chem. A* **2002**, *106*, 5510.
(77) Duschinsky, F. *Acta Physicochim. U.R.S.S.* **1937**, *7*, 551.
(78) Herzberg, G.; Teller, E. *Z. Phys. Chem. B* **1933**, *21*, 410.
(79) Bunker, P. R.; Jensen, P. *Molecular Symmetry and Spectroscopy*, 2nd ed.; NRC Research Press: Ottawa, 1998.
(80) Zwier, T. S.; Carrasquillo, M. E.; Levy, D. H. *J. Chem. Phys.* **1983**, *78*, 5493.
(81) Syage, J. A.; Felker, P. M.; Zewail, A. H. *J. Chem. Phys.* **1984**, *81*, 4685.
(82) Urano, T.; Hamaguchi, H.; Tasumi, M.; Yamanouchi, K.; Tsuchiya, S.; Gustafson, T. L. *J. Chem. Phys.* **1989**, *91*, 3884.
(83) Takahashi, M.; Kimura, K. *J. Phys. Chem.* **1995**, *99*, 1628.
(84) Ansbacher, F. *Z. Naturforsch.* **1959**, *14a*, 889.
(85) Lewis, J. D.; Malloy, T. B., Jr.; Chao, T. H.; Laane, J. *J. Mol. Struct.* **1972**, *12*, 427.
(86) Pitzer, K. S.; Gwinn, W. D. *J. Chem. Phys.* **1942**, *10*, 428.
(87) Albrecht, A. C. *J. Chem. Phys.* **1960**, *33*, 156.
(88) Berkowitz, J. *Photoabsorption, Photoionization and Photoelectron Spectroscopy*; Academic Press: New York, 1979.
(89) Western, C. M. PGOPHER, a Program for Simulating Rotational Structure; University of Bristol; http://pgopher.chm.bris.ac.uk.
(90) Marquardt, D. W. *J. Soc. Ind. Appl. Math.* **1963**, *11*, 431.
(91) Reich, J.-G. *C curve fitting and modelling for scientists and engineers*; McGraw-Hill: New York, 1992.
(92) McCullough, J. J. *Can. J. Chem.* **1968**, *46*, 143.
(93) Palensky, F. J.; Morrison, H. A. *J. Am. Chem. Soc.* **1977**, *99*, 3507.
(94) Giacherio, D.; Morrison, H. *J. Am. Chem. Soc.* **1978**, *100*, 7109.
(95) Padwa, A.; Goldstein, S.; Loza, R.; Pulwer, M. *J. Org. Chem.* **1981**, *46*, 1858.
(96) Morrison, H.; Giacherio, D.; Palensky, F. J. *J. Org. Chem.* **1982**, *47*, 1051.
(97) Felker, P. M.; Baskin, J. S.; Zewail, A. H. *J. Phys. Chem.* **1986**, *90*, 724.
(98) Felker, P. M.; Zewail, A. H. *J. Chem. Phys.* **1987**, *86*, 2460.
(99) Baskin, J. S.; Felker, P. M.; Zewail, A. H. *J. Chem. Phys.* **1987**, *86*, 2483.
(100) Baskin, J. S.; Zewail, A. H. *J. Phys. Chem.* **1989**, *93*, 5701.
(101) Felker, P. M. *J. Phys. Chem.* **1992**, *96*, 7844.